

12-2014

## Low speed water tunnel testing

John J. Taylor  
*University of Texas-Pan American*

Follow this and additional works at: [https://scholarworks.utrgv.edu/leg\\_etd](https://scholarworks.utrgv.edu/leg_etd)



Part of the [Mechanical Engineering Commons](#)

---

### Recommended Citation

Taylor, John J., "Low speed water tunnel testing" (2014). *Theses and Dissertations - UTB/UTPA*. 978.  
[https://scholarworks.utrgv.edu/leg\\_etd/978](https://scholarworks.utrgv.edu/leg_etd/978)

This Thesis is brought to you for free and open access by ScholarWorks @ UTRGV. It has been accepted for inclusion in Theses and Dissertations - UTB/UTPA by an authorized administrator of ScholarWorks @ UTRGV. For more information, please contact [justin.white@utrgv.edu](mailto:justin.white@utrgv.edu), [william.flores01@utrgv.edu](mailto:william.flores01@utrgv.edu).

LOW SPEED  
WATER TUNNEL TESTING

A Thesis

by

JOHN J. TAYLOR

Submitted to the Graduate School of  
The University of Texas Pan American  
In partial fulfillment of the requirements for the degree of

MASTER OF SCIENCE

December 2014

Major Subject: Mechanical Engineering



LOW SPEED  
WATER TUNNEL TESTING

A Thesis  
by  
JOHN J. TAYLOR

COMMITTEE MEMBERS

Dr. Robert Freeman  
Chair of Committee

Dr. Isaac Choutapalli  
Committee Member

Dr. Horacio Vasquez  
Committee Member

December 2014



Copyright 2014 John J. Taylor

All Rights Reserved



## ABSTRACT

Taylor, John J., Low Speed Water Tunnel Testing. Master of Science (MS), December, 2014, 56 pp., 5 tables, 32 figures, 13 references.

Water tunnels are ideal for studying flow patterns for hydrodynamic effects. The functionality of the University of Texas-Pan American water tunnel was limited by not being able to measure forces and moments corresponding to flow patterns. This report delivers an experimental set-up for calibrating the velocity of the water and development of a load measuring system to relate simultaneous visual investigation. An in-depth parts breakdown of the SST-model pump and the dye injection system for flow visualization will be reviewed. Few balances have been made for water tunnels due to small and difficult to measure flow-induced forces. The motive is to interpret the coincident load measurement to the observed flow behavior. The UTPA aerodynamic laboratory has developed a multi-component strain-gauge force balance measurement system for its water tunnel. This setup, in its entirety, is able to relate the velocity of the flow to the measured forces and visual flow patterns.





## DEDICATION

I thank God for guiding me to complete my thesis studies and dedicate this paper to my mom, Edna Taylor, my dad, Edgar Taylor, my brother, Francis Taylor, and all my family including my grandparents, Edgar Alfred Taylor Sr., Jessie Taylor, Francisco Ornelas Cuellar (FOC), and Romelia Ornelas. Thank you for your love and support and helping me get through day by day.



## ACKNOWLEDGMENTS

Thank you Dr. Robert Freeman, Dept. Chair., Dr. Isaac Choutapalli, and Dr. Horacio Vasquez for being on my committee and helping me with everything anybody could ever think of. Thank you Dr. Bob Jones, Dr. Constantine Tarawneh, Dr. Young-Gil Park, and Dr. Kevin Lee for their advice and expertise. Thank you Hector, Alfonso Salinas, Kevin, JR, and Andres for helping me in the highbay and getting your hands dirty. Thank you Kurt Banaszynski from Engineering Laboratory Design (ELD); Carol Zurhellen from Omega Engineering; Mr. Don Lamp with Locke Well & Pump; Tom Benson NASA Engineer; Rio Grande Valley Plumbing Supply; Rubber & Gasket Company of America McAllen, TX;



## TABLE OF CONTENTS

	Page
ABSTRACT .....	iii
DEDICATION .....	iv
ACKNOWLEDGEMENTS .....	v
TABLE OF CONTENTS .....	vi
LIST OF TABLES .....	viii
LIST OF FIGURES .....	ix
CHAPTER I. WATER TUNNELS .....	1
University of Texas Pan American Water Tunnel .....	4
Components of the Water Tunnel at UTPA.....	6
Fluid Circuit Component Descriptions .....	6
General .....	6
Construction .....	7
G&L Model SST Pump .....	8
Installation/Assembly Procedure .....	12
CHAPTER II. WATER TUNNEL CALIBRATION .....	14
Experimental Setup .....	15
Transducer .....	15
Pitot Tube .....	20
Results .....	21

CHAPTER III. FORCE MEASUREMENT .....	24
Literature .....	24
Testing Assembly .....	26
Balance Design Concept .....	27
Wheatstone Bridges and Strain Gauges .....	28
Strain Gauge Installation .....	33
Signal Conditioning Setup .....	36
Calibration Matrix .....	41
CHAPTER IV. CONCLUSION .....	43
Future Work .....	43
REFERNCES .....	45
APPENDIX A .....	46
BIOGRAPHICAL SKETCH .....	56

## LIST OF TABLES

	Page
Table 1: Properties of water and air at 20°C and standard atmospheric pressure .....	3
Table 2: Dimensionless groups when testing models .....	4
Table 3: Parts ordered from Locke Well & Pump .....	12
Table 4: SGD series specifications .....	37
Table 5: Matrix for external rotary side switches .....	40





## LIST OF FIGURES

	Page
Figure 1: Water tunnel at the University of Texas Pan American .....	5
Figure 2: 6” dye model set .....	6
Figure 3: Left-side view of rust around the leak-hole.....	9
Figure 4: Front view of the adaptor and shaft .....	9
Figure 5: Rust on interior side of the casing .....	10
Figure 6: Worn mechanical sleeve.....	11
Figure 7: Fractured mechanical seal .....	11
Figure 8: PX2300 differential pressure transmitter .....	17
Figure 9: 2-wire loop diagram .....	18
Figure 10: PX2300 wire connection ports .....	18
Figure 11: PX2300 wet differential pressure transmitter mounted on frame .....	19
Figure 12: Bleed screws on PX2300 .....	20
Figure 13: Pitot tube installed in water tunnel .....	21
Figure 14: Voltage vs. frequency of motor .....	22
Figure 15: Pressure differential vs. voltage .....	22
Figure 16: Velocity vs. frequency of motor .....	23
Figure 17: Diagram of model support assembly .....	25
Figure 18: Detailed picture of assembly .....	25

Figure 19: Delta wing aircraft attached to C-Strut with dye tubes .....	26
Figure 20: Quarter-bridge type I circuit diagram .....	29
Figure 21: Half-bridge type I circuit diagram .....	30
Figure 22: Half-bridge type II circuit diagram .....	30
Figure 23: Full-bridge type I circuit diagram .....	32
Figure 24: Full-bridge type II circuit diagram .....	33
Figure 25: Strain gauge mounted on attachment cylinder .....	35
Figure 26: Strain gauge visual representation .....	37
Figure 27: Isometric view of BCM-1 .....	38
Figure 28: 1/4-Bridge 120 $\Omega$ Hook-up .....	38
Figure 29: 1/4-Bridge 350 $\Omega$ Hook-up .....	38
Figure 30: 1/2-Bridge 120 $\Omega$ Hook-up .....	38
Figure 31: Visual representation and wire diagram of the DMD-4059 .....	39
Figure 32: Block diagram of measuring system .....	41

## CHAPTER I

### WATER TUNNELS

A water tunnel is an experimental facility used for testing hydrodynamic behavior of submerged bodies in flowing water. Very similar to a recirculating wind tunnel, a water tunnel can replicate data and give realistic flow visualization. There are many kinds of aerodynamic experimental facilities containing a wide variety of tunnels including; low/high speed wind, cavitation, open circuit, closed circuit, free-flight, propeller, propulsion, icing, pressure, and transonic and supersonic tunnels, among others. For many cases, the Reynolds number ( $Re$ ), which is a dimensionless quantity defined as the ratio of inertial forces to viscous forces, dictates whether the results will be comparable between working fluids. Today, around 100 years after the first successful airplane, there is a wide variety of aircraft tailored for specific uses corresponding to their shape. The invention, use and ongoing investigation of the water tunnels has and is now motivated by a wide interest in practical situations in aerodynamics and the fact that theoretical and computational methods are not sufficient to provide the full range of results needed to guide detailed design decisions. It should be noted that any aerodynamic design problem should be based on application of a combination of experimental, theoretical, and computational methods. Scientists often dispute between the small, simple, cheap, accessible experiment, on one hand, and elaborate, detailed, complex, expensive apparatus, on the other. It would be accurate to say that each experimental apparatus enjoys its place in the spectrum from

exploratory investigation of fundamentals to advanced and detailed engineering design. With this in mind, it is possible to find a very favorable niche for water tunnels. Generally speaking, water tunnels belong to the first category where most can be found at university facilities as opposed to the more complete, in-depth experimentally designed water tunnels of government and industry installations [4]. These machines are easily operated and maintained, with minimal environmental impact and electrical power requirements typically less than 50kW, safety concerns are minimal, and facility availability is ideal. Other advantages water tunnel models have over wind tunnels are faster build times, less expense, and they can be more easily modified to satisfy the desired testing conditions. Primarily, water tunnels have been used for detailed flow-visualization studies testing scaled models, such as aircrafts. These studies are better suited for water tunnels than for wind tunnels because the dye that can be injected has higher density and lower mass diffusivity than the water meaning potentially less turbulence and better flow visualization quality. In reality, the free-stream velocities used in water tunnels are substantially less than those in wind tunnels. Flow-visualization is the art of making flow patterns visible, which can give insight into the complex flow behavior around models, allowing scientists and researchers to understand the dynamics of fluid flow. With the development of pressure-transducer and strain-gauge-balance technologies, it is possible to measure accurately the infinitesimal flow-induced pressures, forces, and moments on models in water tunnels. Being able to measure the loads while simultaneously visualizing flow patterns makes it possible to correlate them directly. This technology has increased the usefulness of water tunnels. Although like any facility, water tunnels are not a low cost solution to complex engineering problems. They are compromised by limitation to low Reynolds numbers and Mach-numbers. Also, further complications rise in dealing with water, such as corrosion, leaks and water specifications where

filters are involved, etc. One should realize the important role testing water tunnels can have in aerodynamics; however, researchers should also be aware of the types of models and analyses that can be tested and undertaken to achieve meaningful results.

<b>Property</b>	<b>Water</b>	<b>Air</b>	<b>Unit</b>	<b>Water/Air</b>
Density	998.2	1.204	kg·m <sup>-3</sup>	829.1
Dynamic viscosity	1.002 × 10 <sup>-3</sup>	1.813 × 10 <sup>-5</sup>	kg·m <sup>-1</sup> ·s <sup>-1</sup>	55.27
Kinematic viscosity	1.003 × 10 <sup>-6</sup>	1.506 × 10 <sup>-5</sup>	m <sup>2</sup> ·s <sup>-1</sup>	0.0666
Sonic velocity	1482	343.2	m·s <sup>-1</sup>	4.318

Table 1. Properties of water and air at 20°C and standard atmospheric pressure.

Observing table 1 above, one can expect that the differences between the two media, water and air, can affect the research being carried out. For boundary layer studies, properties of water are favorable compared to those for air. The kinematic viscosity is 15 times smaller in water than that of air. For example: in aerodynamic tests, Reynolds numbers are greater in water than in air by a factor of 15 if models are the same size and have the same free stream velocity. Typically wind tunnel testing use substantially larger models and have a significantly higher free-stream velocity than water tunnel testing. For low speed applications, water tunnels are better suited when hydrodynamic forces are involved and clearer flow visualization is sought. When models are tested in tunnels, it is necessary to satisfy similarity requirements so the tests are representative of full-size practicality. There are three parameters for similarity: geometric, kinematic, and dynamic similarity. As for scaling or dimensions, the model must have the same shape as the full-size, so the dimensions have a constant ratio. For kinematic similarity, velocities at locations in the flow field must have a constant ratio. For dynamic similarity, forces at corresponding locations must have a constant ratio. Table 2 below covers dimensionless groups commonly used in fluids applications like the one in this thesis.

Dimensionless Group	Name	Interpretation	Types of Applications
$\frac{\rho U D}{\mu}$	Reynolds number, $Re$	<u>inertia force</u> viscous force	All types of fluid-dynamics flows
$\frac{U}{a}$	Mach number, $M_1$	<u>flow speed</u> speed of sound <u>inertia force</u> compressibility force	Flows in which compressibility is important
$\frac{\omega D}{U}$	Strouhal number, $St$	<u>wavelength</u> length scale <u>inertia (local) force</u> inertia (convective) force	Unsteady flows with a characteristic frequency of oscillation
$\frac{U}{\sqrt{gD}}$	Froude number, $Fr$	<u>inertia force</u> gravitational force	Flows with a free surface
$\frac{\rho U^2 D}{\sigma}$	Weber number, $We$	<u>inertia force</u> Surface-tension force	Flows in which surface tension is important

Table 2. Dimensionless groups when testing models [6]

### University of Texas Pan American Water Tunnel

The University of Texas Pan American water tunnel, provided by Engineering Laboratory Design (ELD), model 503-30 cm is shown in Figure 1. The details and specifications of the water tunnel will be discussed in this section. The broad specifications for this water tunnel include a maximum flow velocity of 1 m/s; a test section of dimensions 30cm x 30cm x 100cm; overall dimensions of 5.35m x 169.0cm x 183cm; mass of 3700 kg when it is full of water, and it has two 15 hp motors driving the two water circulation pumps. This water tunnel was installed by ELD in 1995. [ELD]

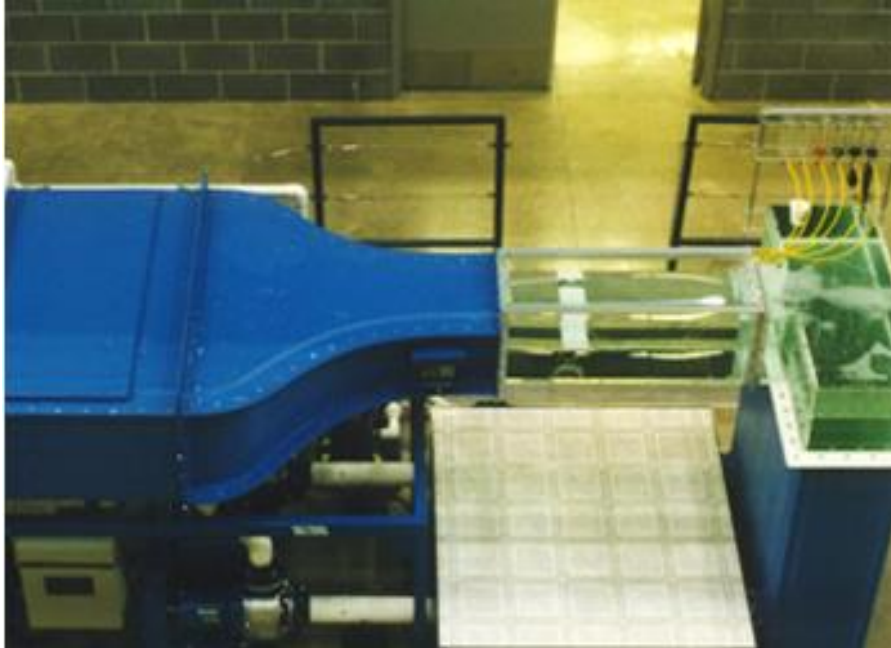


Figure 1. Water tunnel at the University of Texas Pan American.

Add-ons to the ELD water tunnel models include; (1) NACA 0012 and 4412 airfoils with multiple dye taps; (2) flat plate; (3) cylinder models; (4) smooth sphere; (5) hemispherical cup; (6) streamlined body; (7) chamfered circular disk; and (8) dye stream injector with ruler as shown in figure 2.





Figure 2. 6" dye model set

### **Components of the Water Tunnel at UTPA**

The diagrams for the water tunnel are shown in Appendix A. Problems arising from leaks, proper assembling of the SSH-model pump, and circuit components will be thoroughly discussed in this section. First, in order to safely use the water tunnel, one major and some minor leaks needed to be fixed for the water circulation to be controlled and to meet safety requirements in the high bay area.

### **Fluid Circuit Component Descriptions**

**General.** The system is a recirculating design with the flow loop arranged in a vertical configuration. System components include: flow sections, test section, circulating pumps, variable speed drive assembly, piping, supporting framework, working platform, and filtering station. The tunnel has a capacity of approximately 2,625 liters of water.

**Construction.** The sectors holding the water are fabricated of a composite lamination of fiberglass reinforced plastic and a rigid PVC foam core. The foam core essentially is a strong, lightweight structure that easily withstands the static and dynamic loads imposed upon it. The foam also serves as a thermal insulator and significantly reduces condensation. The interior of the composite is glass smooth gel-coat, and the exterior surfaces are spray on blue, polyester, gel-coat enamel. Flanged joints connecting the sectors are sealed using a high quality polyurethane marine adhesive sealant. It is important to insure the alignment of mating sections to eliminate discontinuities that would potentially disturb the flow. A perforated cylinder distributes flow to the distribution chamber. Downstream from the test section, a turning vane system in the return plenum divides the flow into the return plenum reservoir. The top portion of the return plenum is made of transparent plexiglass for visual observation.

The test section is made of 19.05mm Super Abrasion Resistant ® clear acrylic plexiglass. The interior dimensions of the test sections are 30.0cm wide by 37.5cm high by 100.0cm long. Upstream of the test section and preceding contraction is an extended length plenum with flow management components. Including here are a 7.62cm long, precision round cell polycarbonate plastic honeycomb section, three stainless steel plates, and four highly porous stainless steel screens. The flow sections are held together with a single frame fabricated of steel tubing joined by welding. Each frame leg has an adjustable leveling pad. Commercial PVC pipe is used throughout the tunnel. There are two commercially available, *G&L Model SST 3x4-8, 8 7/16* pumps. Each pump is belt driven by a 7.5 HP, ODP, 1800RPM, 208-230 VAC, 3phase, 60Hz motor (*Toshiba Model No. BY75DLF2USH01*). A remote control station located adjacent to the test sections regulates the test section flow velocity. One pump is provided with a separate disconnect to allow only one pump to be operated at a time for lower range velocities. When in

operation, the dye injection system will pollute and color the water. A commercial filter system is provided to remove the dye concentrations and other contaminants from the system water. The filter system is comprised of a 1/2HP circulating pump (*G&L Model No. NPE 1x1.25-4, 4 7/16 Catalog No. 1<sup>ST</sup>2C2E4*), replaceable activated carbon particle filter cartridges, and PVC piping leading back into the top of the inlet plenum chamber. The approximately 2,600 liters of water can be filtered in just one hour. The water tunnel is accompanied by a working platform 38.5cm high to provide easier access through the test section ceiling.

### **G&L Model SST Pump**

Prior to this research, the water tunnel was physically relocated in the high bay of the engineering building. Numerous leaks arose throughout the water tunnel due to this relocation. To repair the water tunnel, required fixing a number of different components. The test area needed to be scraped and re-caulked along the entire perimeter and within the bolts that connect the test area to the return and distribution plenums. A drainage piping system had to be re-designed to adequately drain all the water to the appropriate drain. (This task took no more than a couple 90° elbows and some added PVC piping) Furthermore, flanges needed to be replaced accompanied with custom made four-inch diameter rubber gaskets to replace the original gaskets. A combination of stress relaxation on the rubber and high pressures caused water to leak through and cause rust corrosion on the gaskets. Most importantly, this section covers the diagnosing and repair of the leak in pump #2. Figure 3 pictures the rust from the leak-hole developed after many years. Following, is figure 4 displaying the water line on the adaptor. It should be noted that there should not be any water in contact with the adaptor. The rustic water

between the adaptor and the stainless steel casing consequently rusted the interior of the casing shown in figure 5.



Figure 3. Left-side view of rust around the leak-hole.



Figure 4. Front view of the adaptor and shaft.



Figure 5. Rust on the interior side of the casing

The impeller was taken off with a gear puller carefully so as not to bend the fins and alter the rotational moment of inertia. Once the impeller and adapter were removed it was evident that the rotary seal had worn the shaft sleeve. The bearings and shaft were disassembled using a one-ton hydraulic press. The worn shaft sleeve needed to be taken off by “turning down” on the lathe where after a nice polishing of the shaft was necessary. Figure 6 below shows exactly where the wear occurred on the sleeve.



Figure 6. Worn mechanical sleeve

The mechanical seal or rotary seal acts as a check valve and a slider bearing. The function of the check valve is to prevent liquid under pressure from leaking out of the pump [13]. Figure 7 below shows the fractured rotary seal.



Figure 7. Fractured mechanical seal

The pump, as stated earlier, is “commercially available enclosed impeller all stainless steel construction, centrifugal pumps are used (*G&L Model No. SST 3x4-8, 8 7/16 Catalog No. 23STFRMC0*). Pump case impeller and shaft are fabricated of 316 stainless steel.” Each pump is belt driven by a 7.5 HP, ODP, 1800 RPM, 208-230 VAC/3phi/60Hz motor. To finalize repair of the pump, the following parts in Table 3 were ordered from Lockwell & Pump Co. Located in Appendix A is the ”Pump End Parts for Close Coupled or Frame Mounted Configuration.” And a catalog subjected: Item number, Part description, material.

Part #	Part Name	Description	Cost
126	Shaft Sleeve	4K262	\$117.00
178	Impeller Key	4K261	\$9.10
198	Impeller Bolt	13K155	\$11.00
383	Mechanical Seal	10K16	\$96.00
383A	Seal Spring Retainer	4L216	\$13.00
428	Impeller Gaskets	5L74	\$9.00 each
Total			\$261.10+\$55.00 S&H

Table 3. Parts ordered from Locke Well & Pump

### **Installation/Assembly Procedure**

Prior to re-installing the pump, it was deemed necessary to further prepare numerous parts. Polish the shaft, and remove all rust off parts with a wire wheel until smooth and shiny; scrape the adhesives off the adaptor, and fix the rusty bolts. Typically, according to Locke Well & Pump co., the pump should be assembled as shown in the diagram in Appendix A,

respectively from right to left. Using a one-ton press machine, hydraulically press the bearings (facing out) onto the shaft and place the sub-assembly into housing. Insert the stationary seal onto casing, and mount the casing onto the adapter with a heavy bead of silicone. Let stand while still applying pressure. Spray high tack adhesive sealant onto the mechanical seal and situate the shaft sleeve and mechanical seal joining to the stationary seal. Then, hydraulically press the impeller with the impeller key onto the shaft all the way. Insert wear ring and tighten the remaining 8 bolts to secure the housing.



## CHAPTER II

### WATER TUNNEL CALIBRATION

Setting the speed of the velocity of the water seems straightforward from the basics of fluid dynamics; however this basic variable engages in a considerable amount of attention for aerodynamicists. Calibration of the water tunnel is necessary to determine the velocity as a function of pressure differential. Velocity is needed to calculate dimensionless groups listed in Table 2; for example, Reynolds number, relates inertia and viscous forces for a particular model based on characteristic length. Calibration can generally be carried out by using a pitot-static probe. The probe is used to measure total and static pressures. The most common device for determining the total pressure or total head and static pressure of a stream is the pitot tube [1]. Pitot tubes were invented by Henry Pitot in 1732 to measure flowing velocity of fluids. Typically a “standard” pitot tube senses total head at the orifice. If the pressures from the two orifices (1) total pressure (2) static pressure are connected to a pressure transducer, the pressure differential will be  $P_o - P_s = \frac{1}{2}\rho v^2$  which the velocity may be calculated provided the density. Applying the Bernoulli equation assumes: (1) Fluid incompressible (2) Fluid is inviscid (3) Steady flow (4) Flow along a streamline. The pitot tube is measured at right angles to the flow direction. One cannot insert a pitot tube in the test section to measure dynamic pressure or speed along with an object under test because the test object will cause changes in the flow. These changes are referred to as “induced flow.”

## Experimental Setup

The pitot-tube, fabricated at the aerodynamic laboratory in UTPA, is of brass material with 0.25" I.D. and 0.4" O.D. The perpendicularity is taken care of by a ¼" 24 threads per inch FTP 90° brass elbow that connects the rod parallel with the flow reading the total pressure, and the perpendicular rod leading outwards through the wall-plug. The total pressure and static pressure tubes are connected to ¼" 27 NPT female brass plugs. Attaching to the brass plugs are clear PVA tubing carrying the pressure to the other end of the tubing to ¼" 27 NPT male brass plugs connecting to a pressure transducer.

## Transducer

In order to be confident in choosing the correct transducer, calculations were made to ensure the accuracy of the transducer was suitable for the application. Manipulation of the Bernoulli equation according to the assumptions: (1) Incompressible fluid, (2) Inviscid fluid, (3) Steady flow, and (4) Flow along a streamline was done to obtain the velocity as a function of the pressure differential between the total and static pressure ports.

$$P_o - P_s = \frac{1}{2}\rho v^2 \Rightarrow v = \sqrt{\frac{2(P_o - P_s)}{\rho}}$$

The minimum and maximum velocities were entered into the manipulated Bernoulli equation to get an idea of the pressure differential that will be experienced. As noted earlier the minimum and maximum velocities from the tunnel are;

$$\left\{ \begin{array}{l} v_{min} = 0.015 \frac{m}{s} \\ v_{max} = 0.95 \frac{m}{s} \end{array} \right\}$$

$$(P_o - P_s) = \frac{1}{2} \left( 1000 \frac{kg}{m^3} \right) \left( 0.015 \frac{m}{s} \right)^2 = 0.1125 Pa$$

$$(P_o - P_s) = \frac{1}{2} \left( 1000 \frac{kg}{m^3} \right) \left( 0.015 \frac{m}{s} \right)^2 = 451.25 Pa$$

$$451.25 Pa - 0.1125 Pa = 0.065 psid$$

0.065 *psid* is the differential pressure predicted between the minimum and maximum velocity of the water in the tunnel. Now it is necessary to calculate the accuracy of the transducer from the information provided from the catalog. [7] As listed, Accuracy:  $\pm 0.25\%$  RSS FS; Linearity:  $\pm 0.20\%$  FS; Hysteresis:  $\pm 0.10\%$  FS; Repeatability:  $\pm 0.05\%$  FS. Equations following is the sum of squares method used to calculate the total error in the PX2300 transducer. [9]

$$Error = \sqrt{\left(\frac{0.25}{100} \times 1\right)^2 + \left(\frac{0.1}{100} \times 1\right)^2 + \left(\frac{0.2}{100} \times 1\right)^2 + \left(\frac{0.05}{100} \times 1\right)^2}$$

$$Error = \sqrt{6.775 \times 10^{-5}} = 0.008 psid$$

The expected pressure differential range from the minimum and maximum velocities were compared to the pressure differential error of the transducer to check if the transducer is capable of measuring accurately: ( $0.065 psid > 0.008 psid$ ). This means the transducer is able of measuring pressure differentials around 10 fold of the expected pressure difference. Figure 8 below shows a picture of the PX2300-1DI wet transducer and the dimensions of the size, ports, etc.

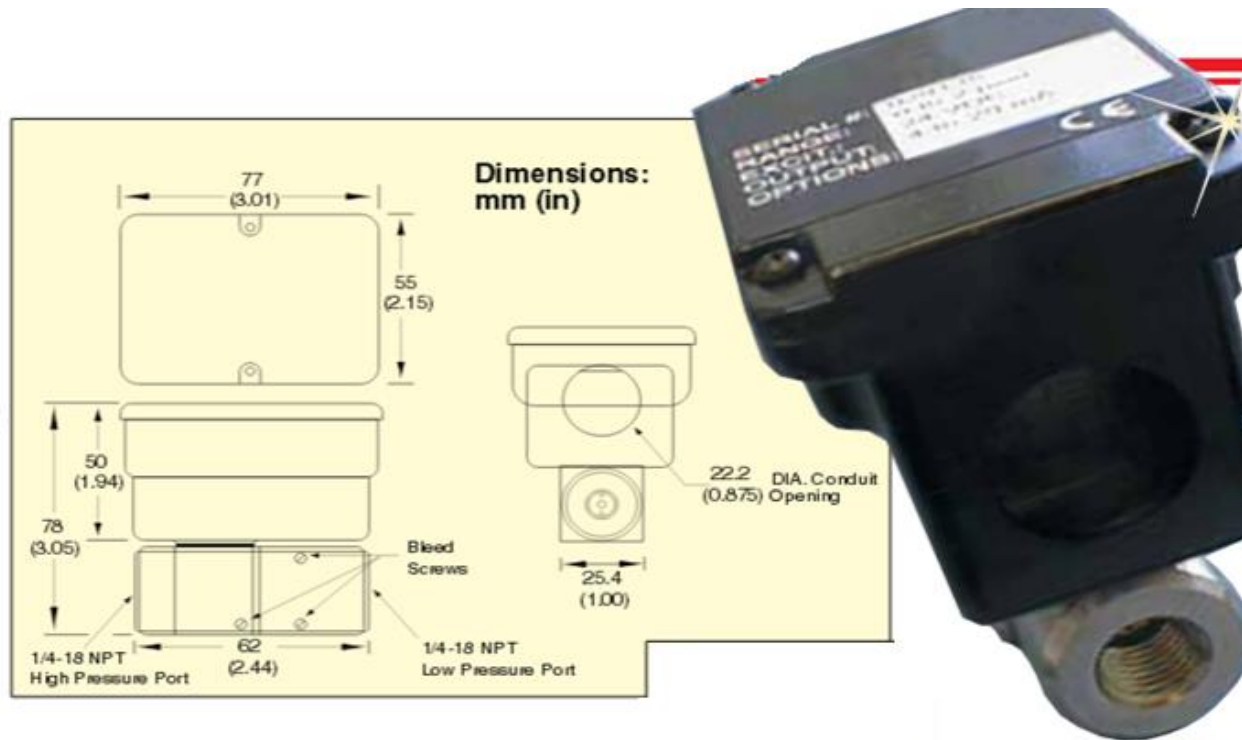


Figure 8. PX2300 differential pressure transmitter. [7]

The current output transmitters are true 2-wire (see figure 9), 4-20mA current devices and deliver rated current into any external load of 0-800 ohms. To access the electrical connections, the cover on top was removed by unscrewing the four screws. Figure 10 shows a diagram of these electrical connections. The PX2300 can operate over a voltage range of 9 to 30 VDC into a 250 ohm load. In this thesis, a 24 VDC was supplied on a 220 ohm load. The PX2300 series comes with 7/8" diameter port intended for a 1/2" I.D. conduit connection.

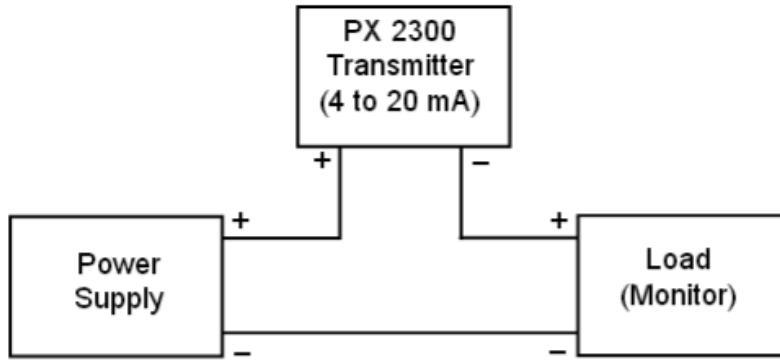


Figure 9. 2-wire loop diagram. [7]

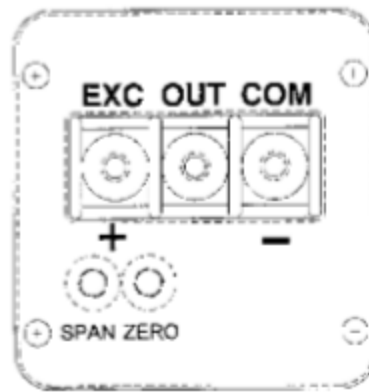


Figure 10. PX2300 wire connection ports. [7]

The PX2300 series is supplied with a mounting bracket and two 6-32 x 3/8 head screws. The mounting bracket was attached below the test section onto the square tube steel frame of the water tunnel. The transmitter was fixed onto the bracket using the two screws and the two tapped holes located on the underside of the transmitter. Figure 11 shows the PX2300 transducer mounted onto the frame. The high and low pressure fittings are standard pipe 1/4"-18 NPT internal fittings. The high pressure port is labeled "High". Brass male 1/4"-18 NPT plugs were purchased to connect the clear tubing to the transducer.

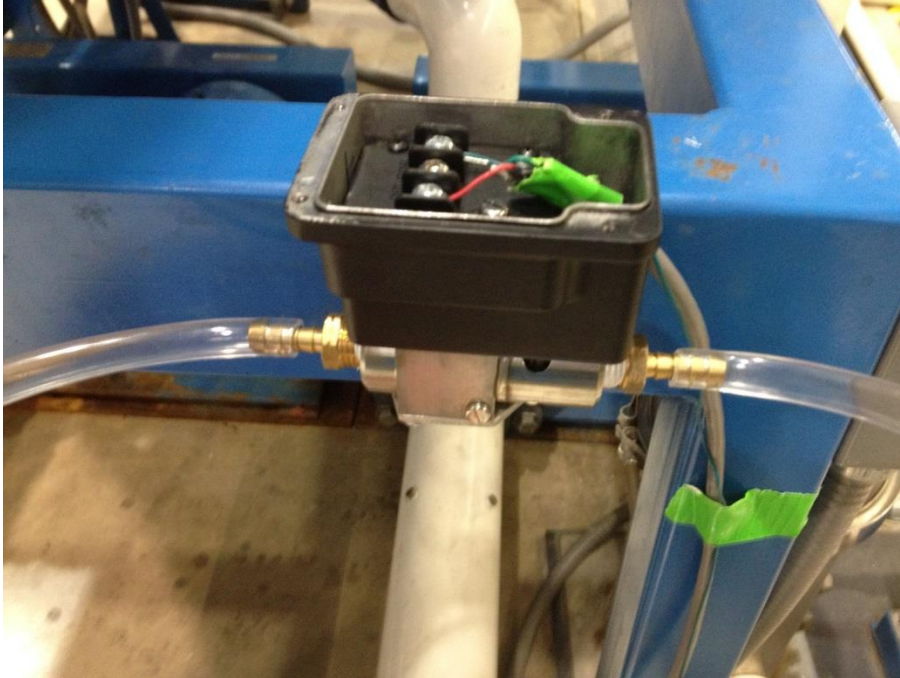


Figure 11. PX2300 wet differential pressure transmitter mounted on frame.

Before taking measurements, it is necessary to bleed the pressure ports to obtain accurate pressure readings. Figure 12 shows a side view of the transducer and its bleed screws. To bleed the pressure ports, back off the first bleed screw mounted on flat side of sensor body (2 turns max) until liquid begins to flow out. Once bubble-free liquid flows out, retighten the bleed screw and repeat the procedure for the second set of bleed screws located on the round section of the low pressure fitting.

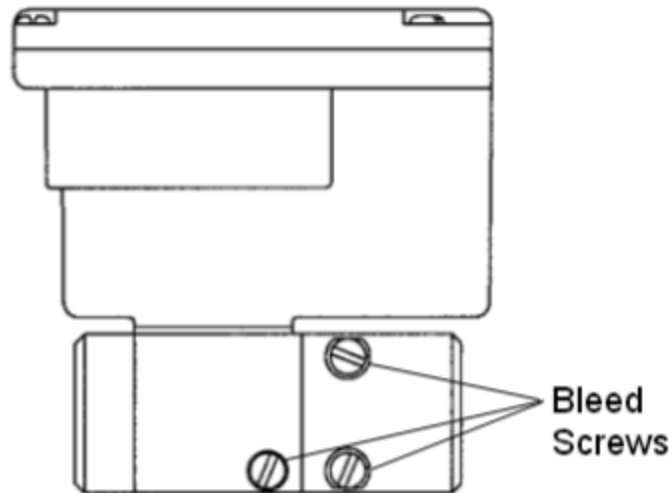


Figure 12. Bleed screws on PX2300

### **Pitot Tube**

The pitot-tube, fabricated at the aerodynamic laboratory in UTPA, is of brass material with 0.25" I.D. and 0.4" O.D. The drawing of the assembly is located in Appendix A. The pitot tube by itself is essentially a three part assembly. The entrance part, parallel to the flow, gradually decreases in diameter 2.5" from the end in a cone-shape to the tip of the probe. A 1/4" NPT female threaded 90° elbow connects the entrance part to the stem. The stem is mounted to the wall plug via pressure fit and epoxy and hardener. On the outside of the wall plug connected to the stem is a brass 1/4" female NPT pressure plug. The static pressure tube is mounted to the wall plug in the same manner; however, to ensure the entrance must be flush with the interior wall of the test section. Figure 13 below is a picture of the pitot tube and static pressure tube mounted on the wall plug in the test section of the water tunnel.



Figure 13. Pitot tube installed in water tunnel.

## Results

Once the hardware for the experimental setup was in place, the test was initiated. The control station adjusts the variable speed motor that regulates the pump shaft RPM. Voltage measurements are taken as the frequency of the motor is operated from 0 to 60 Hz. Figure 14 shows voltage as a function of the frequency of the motor. The PX2300-1DI transducer is a 4-20mA current device proportional to 0 to 1 psid calibrated with a 220 ohm shunt resistor. This data can be interpreted in figure 15. After applying Bernoulli's equation, to finalize the calibration process, the velocity of the water can be obtained as a function of the frequency of the pump shown in figure 16.



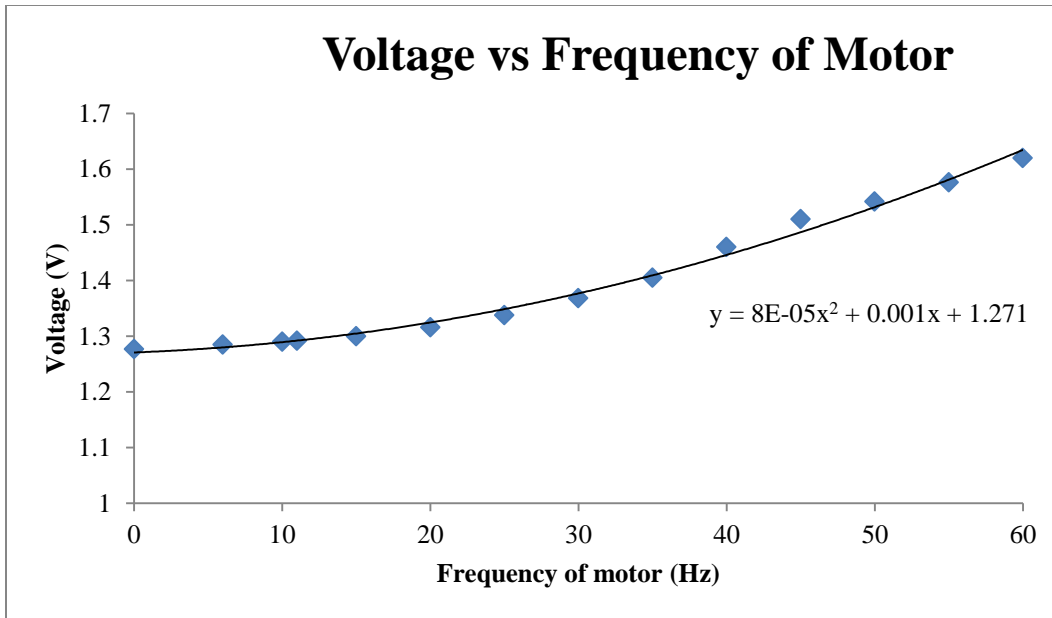


Figure 14. Voltage vs. frequency of motor.

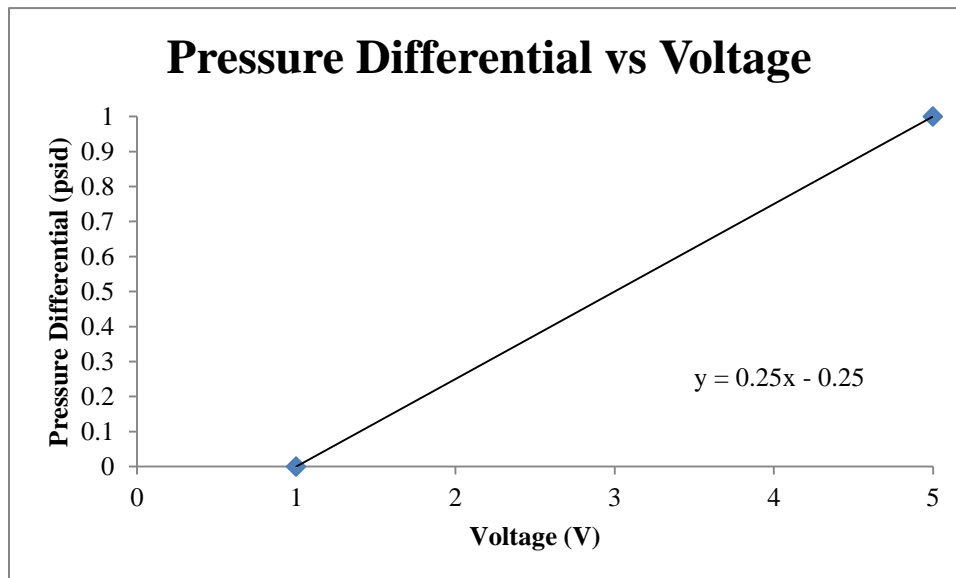


Figure 15. Pressure differential vs. voltage.

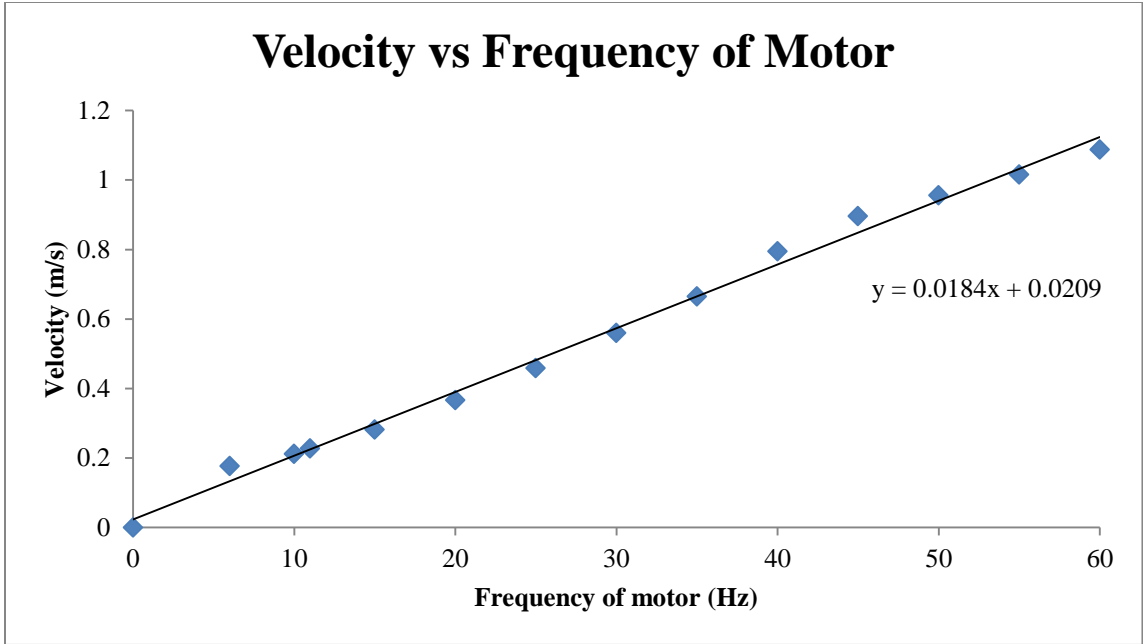


Figure 16. Velocity vs. frequency of motor.

## CHAPTER III

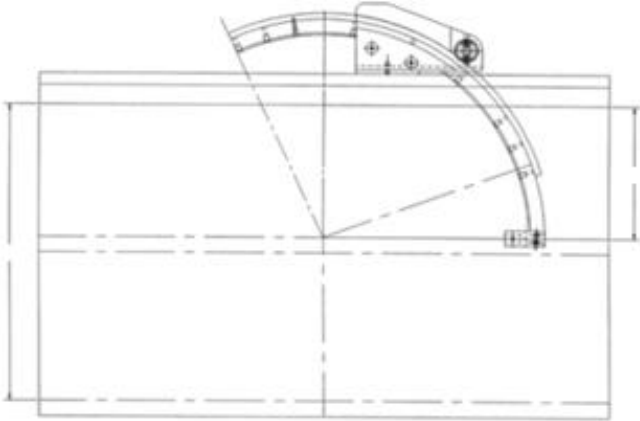
### FORCE MEASUREMENT

Force measurement techniques in water tunnel testing are necessary for determining a variety of aerodynamic performance parameters. These parameters are used to assess the aerodynamic characteristics of a “vehicle” and to guide further design refinements. Typically these techniques rely on static measurement of the reaction forces produced in the model support structure and are designed to minimize balance interactions. [1] As mentioned by Pope et al. (1999), “The purpose of load measurements on the model is to make available the forces and moments so that they may be corrected for tunnel boundary and scale effects and utilized in predicting the performance of the full-scale vehicle.” [1] There are four methods to obtain the loads: (1) measuring the actual forces and moments on the complete model or on parts of the model with multiple balances; (2) measuring stress distribution over the model by using pressure measuring devices through orifices; (3) measure the effect of the model by surveying the wakes and tunnel wall pressures; (4) measuring the motion of model under action of aerodynamic forces and computing forces from equations of motion.

#### **Literature**

“Balance design and use are problems that should not be deprecated; in fact, it might truthfully be said that balance design is among the most trying problems in the field.” [1]

The C-Mount design is in reference to extensive research and previous studies from Rolling Hills Research Corporation. [4] Figures 17,18, and 19 below provide very insightful diagrams and pictures of their C-strut sting mount 1-component testing assembly. [4] This concept was used in designing the testing assembly for UTPA’s water tunnel.



MODEL SUPPORT ASSEMBLY

Figure 17. Diagram of model support assembly. [4]

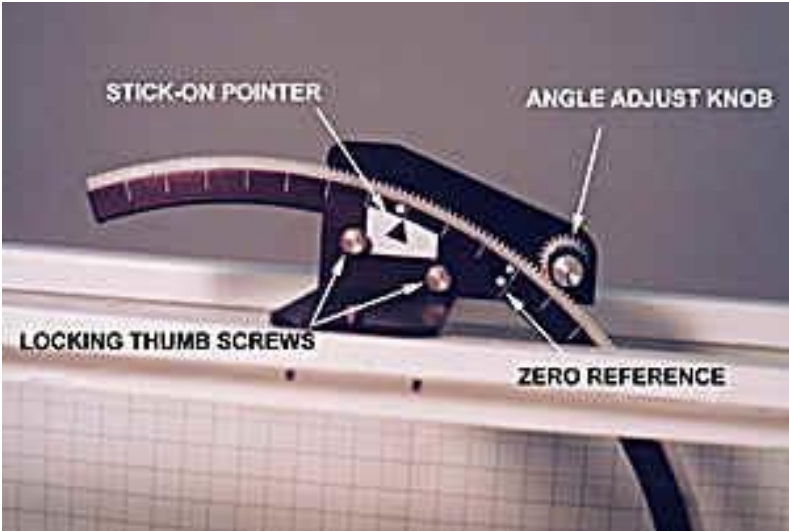


Figure 18. Detailed picture of assembly. [4]

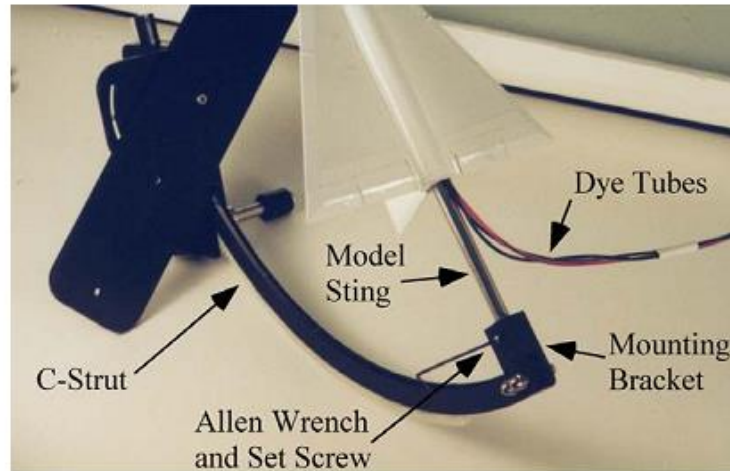


Figure 19. Delta wing aircraft attached to C-strut with dye tubes. [4]

Similar to Rolling Hills Research Corporation, the development of the C-strut, and sting mount must be designed for the UTPA's water tunnel model. Certain design parameters and qualifications were implemented in this project such as: test-section dimensions, including length, width, and height, force compensation, location, complexity, and durability.

The geometric design parameter of the test section was based on the measurements from the diagram in Appendix A. Simple geometry was used to calculate the size of the C-strut in order to maximize the angle of attack to the size constraints of the test section.

### **Testing Assembly**

The testing assembly consists mainly of five parts: (1) sting mount, (2) adapter, (3) C-Strut, (4) attachment cylinder, (5) testing piece. The diagrams for these parts can be found in Appendix A. The sting mount can be described as a rectangular piece that spans the width of the tunnel,  $\frac{1}{4}$  inch thick aluminum and long enough so that the adapter can be mounted in a way for the C-strut. The sting mount attaches to the test section of the water tunnel with c-clamps and is

located as far as possible downstream of the flow. This also enables the user to ensure that the test specimen is centered in the test section of the water tunnel. The adapter is a trapezoidal piece that merely connects the C-strut to the sting mount. The C-strut is guided by an insert screw through a slit held by locking screws to manually fix the C-strut at any angle between  $-45^\circ$  to  $+45^\circ$  from the horizontal. The cylindrical end called the attachment cylinder contains a 6/32" tap that mounts to the C-strut with a bolt. In order to achieve even a higher span of angles of attack roughly an extra ( $\pm 10$  to  $\pm 15^\circ$ ), the user can pivot the attachment cylinder that is attached to the C-strut by loosening the bolt and re-tightening it. An adjustable sting made of 1/4 inch round steel rod, contains the test specimen slides into the attachment cylinder and can be manually adjusted 0-2 inches longitudinally in translation, and a full  $360^\circ$  in rotation. The adjustable sting is secured by a 6-32 set screw. Each experiment that uses this mount, must come with its own adjustable attachment cylinder.

This design was fabricated in the machine shop in the engineering building at UTPA. It was designed under the requirements of having a design with simplicity and adjustability for class experiments in which the user can simply adjust the angle of attack, the length between the test specimen and the force balance, and roll angle.

### **Balance Design Concept**

The concept used to develop the balance design is the "beam theory" bending principle. Simply, the forces acting on the spring element cause strain on the surface which can be detected by strain gauges. Strain gauges are connected in a Wheatstone bridge configuration where the change in strain (change in length divided by the original length) results in a variation in the strain-gauge's electrical resistance; consequently, producing a particular voltage difference from

the bridge, which can be amplified and measured with a data acquisition system. The strain gauge factor, GF, is defined as the relationship between the changes in resistance compared to the change in length with respect to the original length. Mathematically:

$$GF = \frac{\Delta R/R}{\Delta L/L} \equiv \frac{\Delta R/R}{\epsilon}$$

### **Wheatstone Bridges and Strain Gauges**

In order to understand how the voltage signal from the Wheatstone bridge relates to the strain, strain gauge configuration types must be covered. This section briefly describes different types of strain gauge configurations: quarter-bridge type I,II; half bridge type I,II; and full bridge type I,II. All strain-gauge configurations are based on the concept of a Wheatstone bridge.

According to National Instruments [2], a Wheatstone bridge is an array of four resistive legs, where one or more of these legs can be active sensing elements. From the figures, the Wheatstone bridge is the electrical equivalent of two parallel voltage divider circuits. A physical phenomenon, such as a change in strain or a temperature shift, changes the resistance of the sensing elements in the Wheatstone bridge. The number of active legs in the Wheatstone bridge determines the kind of configuration, for example, quarter-bridge has 1, half-bridge has 2, and full-bridge has all 4 active.

A quarter-bridge type 1 Wheatstone bridge configuration, as shown in figure 20, has a single active strain-gauge element mounted in the principle direction to measure either axial or bending strain. In order to complete the circuit, a passive quarter-bridge resistor (dummy resistor) is required. Temperature variation decreases the accuracy of the measurements.

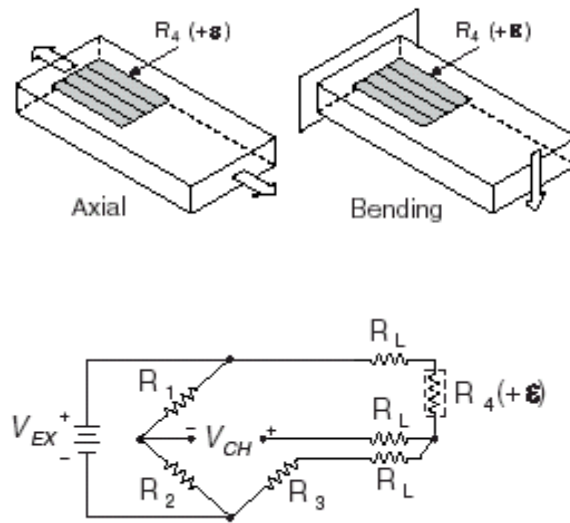


Figure 20. Quarter-bridge type I circuit diagram [2]

R1 and R2 are half-bridge completion resistors, R3 is the quarter-bridge completion resistor or (dummy resistor) and R4 is the active strain-gauge element measuring strain ( $\epsilon$ ). To convert voltage readings to the unit less strain use: where  $R_L$  is the resistance from lead wires.

$$\text{Strain } (\epsilon) = \frac{-4V_r}{GF(1 + 2V_r)} \left(1 + \frac{R_L}{R_g}\right)$$

Half-bridge type I has two active strain-gauge elements. In this configuration, one gauge is mounted in the direction of axial strain and the other acts as a Poisson gauge and is mounted transverse or perpendicular to the principle axis strain. This type compensates for temperature and the aggregate effect. The aggregate effect is a phenomenon that effects the principle strain measurement due to the Poisson's ratio of the specimen material.



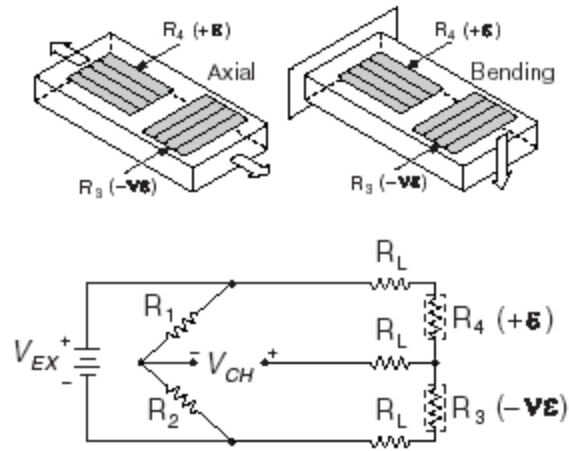
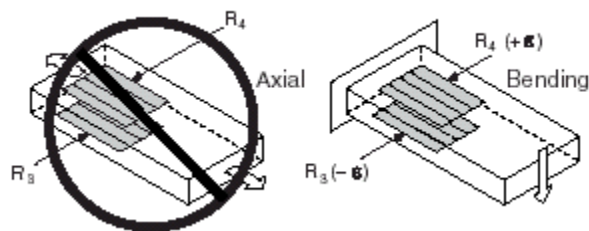


Figure 21. Half-bridge type I circuit diagram. [2]

R1 and R2 are half-bridge completion resistors, R3 is the active strain-gauge element measuring compression from Poisson effect ( $-\nu$ ), and R4 is the active strain-gauge element measuring tensile strain ( $+\epsilon$ ). To convert voltage readings to strain units use:

$$\text{Strain } (\epsilon) = \frac{-4V_r}{GF[(1 + \nu) - 2\nu_r(\nu - 1)]} \left(1 + \frac{R_L}{R_g}\right)$$

Half-bridge type II has two active strain gauges; one is mounted on the top in the direction of bending strain, and the other is mounted on the opposite side (bottom) in the direction of bending strain. This configuration rejects axial strain, compensates for temperature and is sensitive to bending strain.



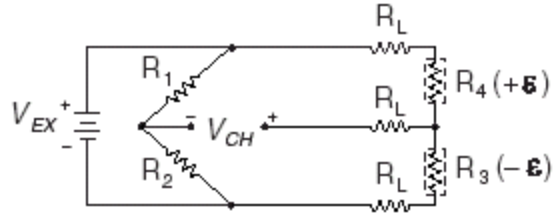


Figure 22. Half-bridge type II circuit diagram. [2]

R1 and R2 are half-bridge completion resistors, R3 is the active strain gauge element measuring compressive strain ( $-\epsilon$ ), and R4 is an active strain-gauge element measuring tensile strain ( $+\epsilon$ ). To convert voltage readings to strain use:

$$\text{Strain } (\epsilon) = \frac{-2V_r}{GF} \left(1 + \frac{R_L}{R_g}\right)$$

Full-bridge type I has four active strain-gauge elements. Two are mounted in the direction of bending strain on one side (top), and the other two are mounted in the direction of bending strain on the other side (bottom). This configuration is highly sensitive to bending strain, rejects axial strain, and compensates for temperature and lead resistance.

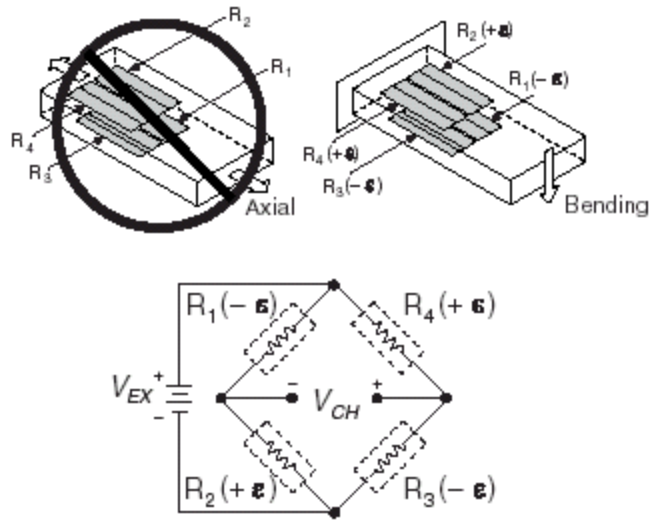


Figure 23. Full-bridge type I circuit diagram. [2]

R1, R2, R3, and R4 are all active strain gauge elements measuring  $(-\varepsilon)$ ,  $(+\varepsilon)$ ,  $(-\varepsilon)$ ,  $(+\varepsilon)$  respectively.

$$\text{Strain } (\varepsilon) = \frac{-V_r}{GF}$$

Full-bridge type II configuration has all four active strain elements. Two are mounted to measure bending strain with one of each gauges on the top and bottom; and the other two are mounted to act together as a Poisson gauge and are mounted transverse (perpendicular) to the principle axis strain with one of each gauges on the top and bottom. This type II bridge rejects axial strain and compensates for temperature while compensating for the aggregate effect by utilizing the Poisson ratio of the material.

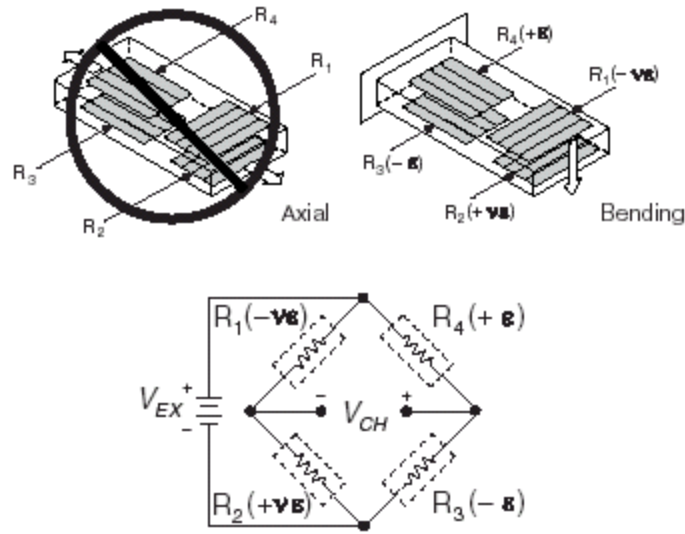


Figure 24. Full-bridge type II circuit diagram. [2]

R1, R2, R3, and R4 are active strain gauge elements measuring compressive Poisson effect ( $-\gamma$ ), tensile Poisson effect ( $+\gamma$ ), compressive strain ( $-\epsilon$ ), and tensile strain ( $+\epsilon$ ) respectively. To convert voltage readings to strain use:

$$\text{Strain } (\epsilon) = \frac{-2V_r}{GF(1 + \nu)}$$

### Strain Gauge Installation

This section will thoroughly cover the proper procedure for installing a strain gauge. There are several steps in preparing the specimen before the strain gauges can be installed. Cleanliness and surface preparations are the key essentials to a successful and working bond. The purpose of surface preparation is to achieve a smooth surface so as to adhere the strain gauge to the specimen.

A coarse cleaning would initially begin the process as to remove any rust, scale, or paint from the location where the strain gauges are to be mounted. This can be done with a coarse grade emery paper. As for this particular scenario, the test specimen has already been cleared of any such contaminants and is ready for smoothing the surface. Vibrations occur during the process from the mill and produce a ‘wavy sunray’ like appearance on the surface of the location on which the gauge needs to be installed. These surface imperfections, or pitting, scratches, protrusions, etc. can be removed by grinding and filing methods. This is followed by using a sand paper with a fine 240 grit followed by a 600 to 1000 grit to achieve a shiny smooth surface that is ready for cleaning. Check to make sure chemical resistance of the material is sufficient so the solvent will not damage it. In this thesis, the material is brass and acetone was used to degrease the surface and wipe clean. Now the test specimen is ready for the bonding procedure [2].

Specific instructions are provided with strain gauge adhesives, Omega [2] provided the cold cure adhesive SG496 (typically used for most metals). When handling the strain gauges, use tweezers to remove them from the package and place onto work surface, typically glass, as to be careful not to touch the gauge for the oils and grease from the skin would contaminate the surface. With the ribbon leads facing up, use cellophane tape to lift the strain gauge from the working surface onto the test specimen. Position the strain gauge in the desired orientation as discussed in section (strain gauge orientation) and secure one end of the tape onto the test specimen. [2] Gently, lift the other end of the tape. When doing this step, the strain gauge assembly will be lifted being careful to not stretch the gauge. Leave the hinge so access is available to the test specimen where the strain gauge position is fixed. Continue with bonding the strain gauge by applying pressure to the top of the gauge until dry and carefully remove the

tape by holding a corner of the strain gauge with a small tool and slightly pulling the tape back. Figure 24 shows strain gauge properly mounted.



Figure 25. Strain gauge mounted on attachment cylinder.

[2] Inspect the strain gauge installation by measuring the base resistance of the unstrained strain gage after it is mounted, but before wiring is connected. Check for surface contamination by measuring the isolation resistance between the gage grid and the stressed force detector specimen using an ohmmeter, if the specimen is conductive. This should be done before connecting the lead wires to the instrumentation. If the isolation resistance is under 500 mega ohms, contamination is likely. Check for extraneous induced voltages in the circuit by reading the voltage when the power supply to the bridge is disconnected. Bridge output voltage readings for

each strain-gage channel should be nearly zero. Connect the excitation power supply to the bridge and ensure both the correct voltage level and its stability. And finally, check the strain gage bond by applying pressure to the gauge. The reading should be unaffected. [2]

### **Signal Conditioning Setup**

Data Acquisition (DAQ) makes it possible for the computer to read the outputs of the strain gauges. Signal conditioning the measurement readings are just as important, if not more important than mounting the strain gauge properly. Without the correct adjustments made, your data acquisition system will give you false interpretations. The concept of obtaining data from the strain gauges is fairly simple with the right tools. This DAQ comprises of a DMD4059 signal conditioner, BCM-1 built in Wheatstone bridge, the strain gauges (of course) type SGD-1.5/120-LY13, and the DAQ (CB-68LP). The following will discuss in detail the specifications and basic instructions.

Strain gauges are available in a wide variety of shapes in sizes. This type SGD-1.5/120-LY13 is used to cover the strain measurement applications. This particular type is rugged and flexible, suitable for highly accurate static and dynamic measurements. The grid is formed by etching constantan foil, which is completely sealed in a medium of polyimide film. This particular strain gauge has a linear pattern, used to measure strain in a single direction typically for experimental stress analysis applications.



Figure 26. Strain gauge visual representation. [3]

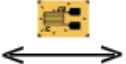
GAGE PATTERN Leads not shown	MODEL NO. Pkg of 10	NOM. RESIS- TANCE ( $\Omega$ )	DIMENSIONS mm (inch) <sup>†</sup>				MAX V* (V <sub>rms</sub> )	TERMINATION
			GRID		CARRIER			
			A	B	C	D		
Shown actual size 4.70 mm  	SGD-1.5/120-LY11	120	1.50 (0.059)	1.20 (0.047)	4.70 (0.185)	3.40 (0.134)	2.5	Ribbon Leads
	SGD-1.5/120-LY13	120	Miniature linear pattern Measurement of stress concentration 120 $\Omega$				3.5	Ribbon Leads
	SGD-1.5/120-LY41	120					2.5	Solder Pads
	SGD-1.5/120-LY43	120	3.5	Solder Pads				

Table 4. SGD series specifications [3].

The strain gauge is then connected by lead wires to a Wheatstone bridge which is built-in to the BCM-1. The Omega BCM-1 bridge completion module is a fairly straightforward tool providing a convenient means to complete the Wheatstone bridge circuit for strain measurements. The BCM-1 is constructed using precision resistors with PPM/ $^{\circ}$ C temperature coefficient for thermal stability. The unit completely encapsulates the resistors that can be used for quarter bridge setups with 120 ohm or 350 ohm gages or half bridges with any resistance. Mounting the BCM-1 is easy with the equipped baseplate. The hook-up figures below show the wire diagram. The hook-up is made using the screw terminals on top of the unit using stripped wires. On one side



there are four terminals for excitation and signal output connections. The excitation voltage is connected to the outer terminals labeled +EX and -EX and the readout device is connected to the center terminals labeled + and - Vout.

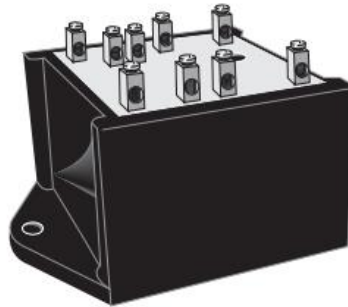
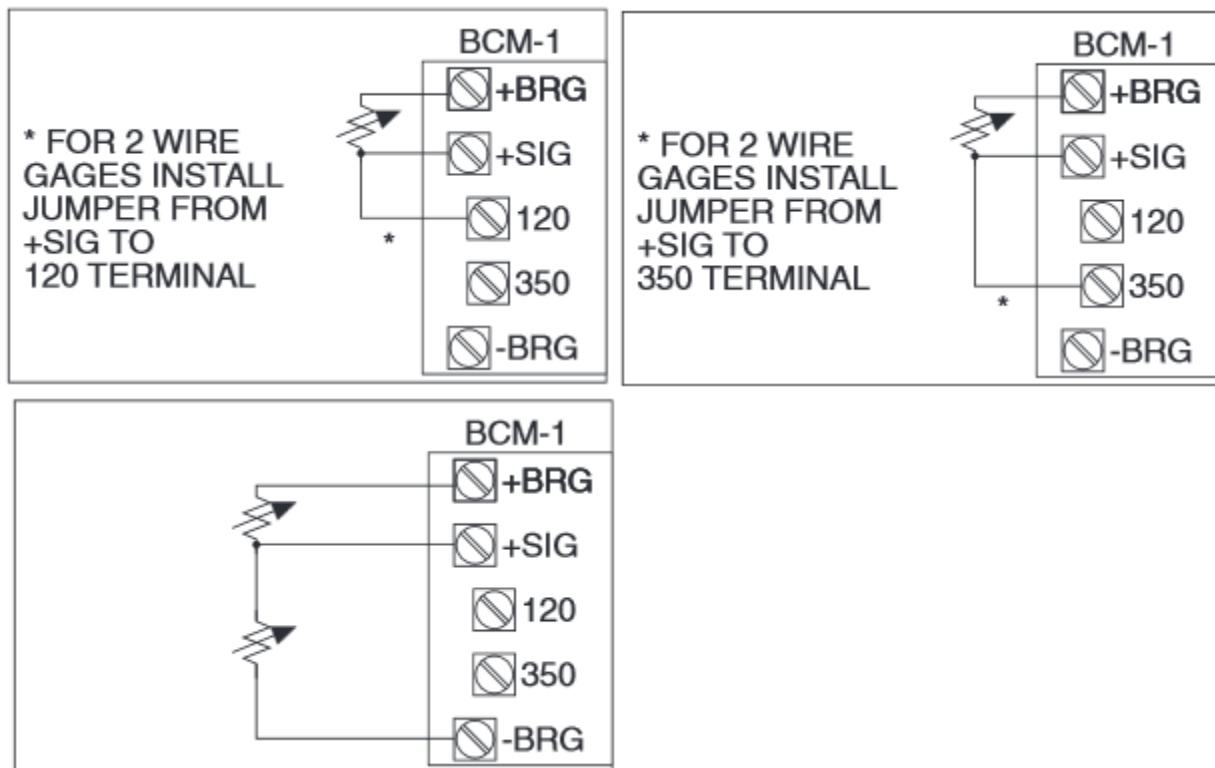


Figure 27. Isometric view of BCM-1



Figures 27-30. 1/4 Bridge 120 Ω; 1/4 Bridge 350Ω; and 1/2 Bridge 120 Ω Hook-up respectively. [2]

The wires leading out from the BCM-1 then connect to the DMD-4059 signal conditioner. It provides a means of filtering, amplifies, and converts the millivolt signal to the selected DC voltage or current output linear to the signal. Input, output, excitation, and zero offset are configurable via external rotary side switches viewable in figure 31.

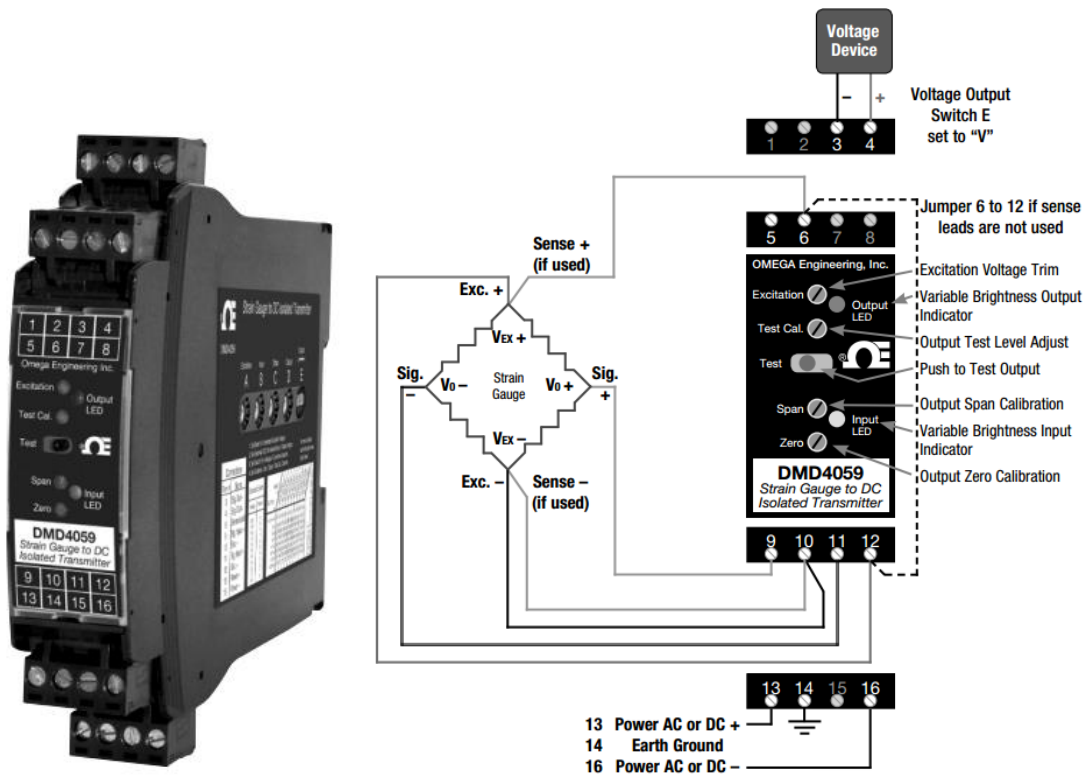


Figure 31. Visual representation and wire diagram of the DMD-4059.

Output	0-1 V	0-2 V	0-4 V	1-5 V	0-5 V	0-8 V	2-10 V	0-10 V	±5 V	±10 V
Switches	BCDE	BCDE	BCDE	BCDE	BCDE	BCDE	BCDE	BCDE	BCDE	BCDE
Input	BCDE	BCDE	BCDE	BCDE	BCDE	BCDE	BCDE	BCDE	BCDE	BCDE
0-5 mV	200V	208V	201V	206V	209V	202V	207V	203V	204V	205V
0-10 mV	A00V	A08V	A01V	A06V	A09V	A02V	A07V	A03V	A04V	A05V
0-20 mV	300V	308V	301V	306V	309V	302V	307V	303V	304V	305V
0-25 mV	600V	608V	601V	606V	609V	602V	607V	603V	604V	605V
0-30 mV	E00V	E08V	E01V	E06V	E09V	E02V	E07V	E03V	E04V	E05V
0-40 mV	B00V	B08V	B01V	B06V	B09V	B02V	B07V	B03V	B04V	B05V
0-50 mV	000V	008V	001V	006V	009V	002V	007V	003V	004V	005V
0-100 mV	800V	808V	801V	806V	809V	802V	807V	803V	804V	805V
0-120 mV	F00V	F08V	F01V	F06V	F09V	F02V	F07V	F03V	F04V	F05V
0-200 mV	100V	108V	101V	106V	109V	102V	107V	103V	104V	105V
0-250 mV	400V	408V	401V	406V	409V	402V	407V	403V	404V	405V
0-300 mV	C00V	C08V	C01V	C06V	C09V	C02V	C07V	C03V	C04V	C05V
0-400 mV	900V	908V	901V	906V	909V	902V	907V	903V	904V	905V

Table 5. Matrix for the external rotary side switches [7].

From the DMD-4059 the signal is transmitted to the DAQ (CB-68LP) provided by National Instruments. [7] Figure 32 below shows a block diagram of the system to obtain raw data that can be interpreted on Labview.

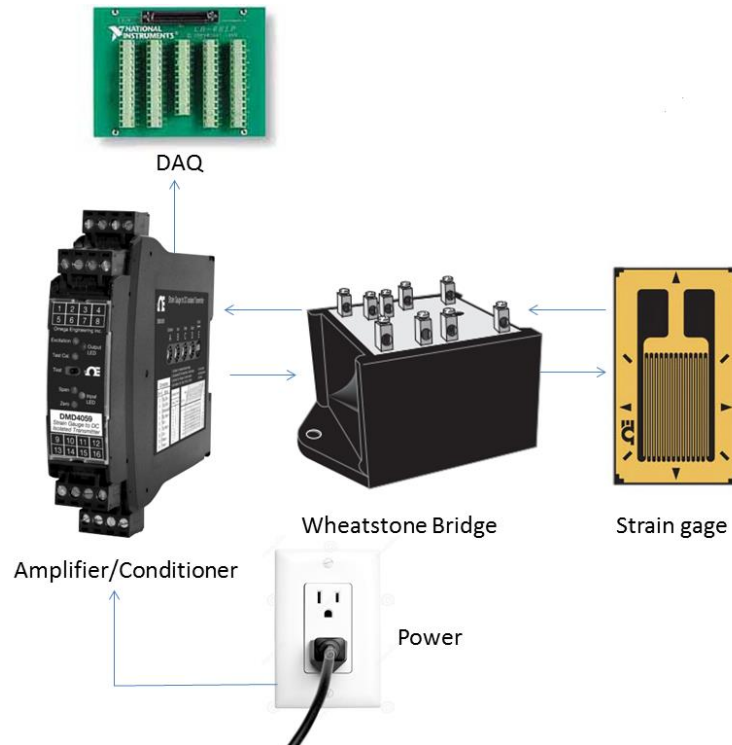


Figure 32. Block diagram of measuring system

### Calibration Matrix

The force balance gives out 2 voltages labeled  $[V_A V_M]$ . A more suitable output is data in the form of forces or moments namely  $[L P]$ . Relating the voltage to a force or moment is completed by taking the data and finding a relationship between the measured value, the voltage, and the known imposed load over several values to give a slope Voltage/Force or Moment. Raw data from the sting balance can be represented by a  $1 \times 2$  matrix of voltages.

$$[V_A V_M]$$

Likewise the desired output vector can be represented as a  $2 \times 1$  matrix of lift force and pitching moment about the fixed plane.

$$[L P]^T$$

When only concerned with first order interactions, raw data can be translated to meaningful measurements with this 2x2 calibration matrix.

$$\begin{bmatrix} m_{L,V_A} & m_{L,V_M} \\ m_{p,V_A} & m_{p,V_M} \end{bmatrix}$$

To determine the entries for this matrix requires loading the balance for each component and observing the output voltages. By applying a series of loads from a low force to a high force, it is possible to obtain a slope for each component. The matrix equation is equal to the transpose of the inversion to find the reverse relationship between voltage and force.

$$[V_A V_M] \left( \begin{bmatrix} m_{L,V_A} & m_{L,V_M} \\ m_{p,V_A} & m_{p,V_M} \end{bmatrix}^{-1} \right)^T = [L P]^T$$

## CHAPTER IV

### CONCLUSION

The goal of this project was to design and develop a calibration system and a multi-component strain gauge sensed force measurement system to relate to the observed flow behavior. However, the force measurement system only accounts for two of the six possible components. The calibration system is comprised of a pitot tube fabricated at the University of Texas Pan American alongside a PX2300 wet pressure transducer. Together the data acquisition system measures the differential pressure between the total and static pressure ports. The velocity of the water was obtained by applying Bernoulli's equation. The uncertainty was calculated based on the standard deviation.

To ensure the safety of the highbay during usage of the water tunnel, repairs were performed to stop all the leaks. The G&L model SST pump was repaired by replacing the failed shaft sleeve, mechanical seal, and stationary seal.

### **Future Work**

To further improve on this work, the force balance needs to measure up to six components. Expand the calibration matrix and range to increase the accuracy and usability of the balance. In order to do so, a jig needs to be designed to apply a pure load to each channel. Once the force balance is capable of measuring up to six components accurately, then testing

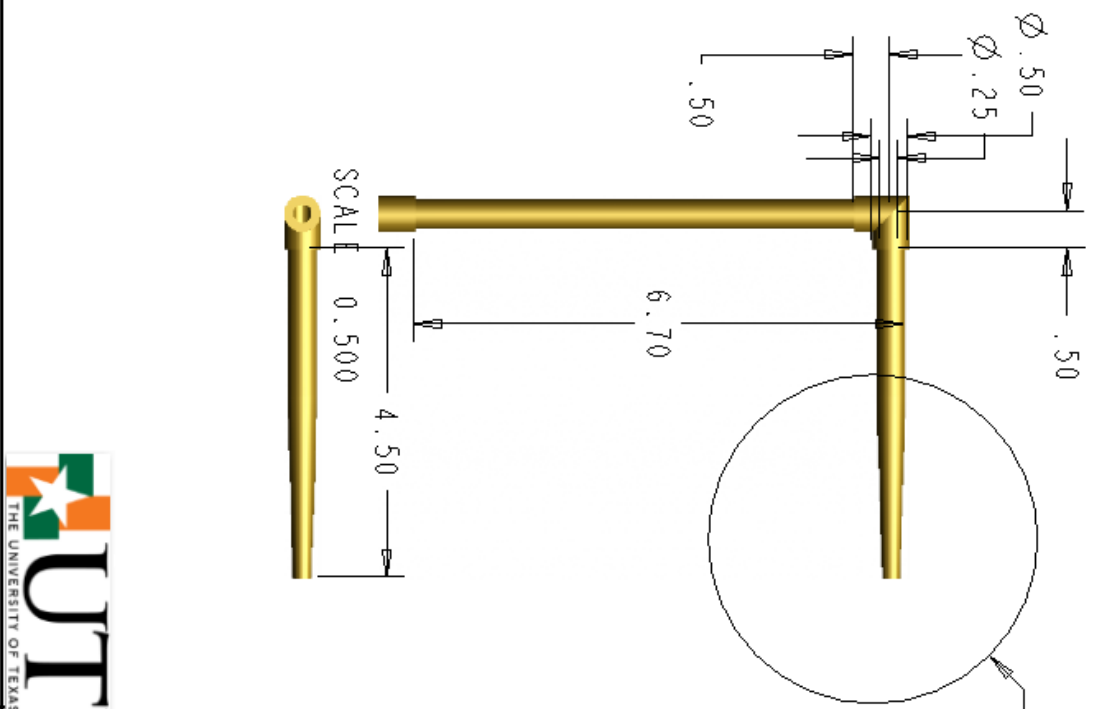
different hydrofoils, aircraft, or submerged objects to compare their aerodynamic characteristics should be analyzed. Upgrade the facility with a particle image velocimetry or other flow visualization measuring apparatus.

## REFERENCES

- [1] “Low Speed Wind Tunnel Testing” A, Pope et.al. Wiley-Interscience; 3 edition (February 22, 1999)
- [2], “Strain Gauge Configuration Types.” *www.Ni.com* ; National Instruments. Publish Date October 6, 2006.
- [3] Omega Engineering. “Pressure strain and force products.” 2013-2014
- [3] “Water Tunnels.” *www.eldinc.com* . Esultants Web Services. 2011
- [4] *www.rollinghillsresearch.com*. Rolling Hills Research Coporation. 2014
- [5] Omega Engineering. Differential Pressure Transducers. Wet/Wet Uni-directional and Bi-directional Ranges.
- [6] Munsen, B. R., Young, D. F. & Okiishi, T. H. 2006 Fundamentals of fluid mechanics, Fifth Edition, John Wiley & Sons, Incorporated.
- [7] Omega Complete Flow and Level Measurement Handbook and Encyclopedia ®, OMEGA Press 1995
- [8] Etkin, B., and Reid, L., Dynamics of Flight, Stability and Control, 3<sup>rd</sup> ed., Wiley, New York, 1996.
- [9] “Error Analysis.” <http://mathforum.org/library/drmath/RMS/erroranalysis>.
- [10] Edwards, A. Virginia Polytechnic Institute. “Comparison of Strain Gage and Fiber Optic Sensors on A Sting Balance In A Supersonic Wind Tunnel.” December, 2000.
- [11] P.A. Aswatha Narayana, K.N. Seetharamu. Engineering Fluid Mechanics. Page 551.
- [12] Wassgren C., Notes on Fluid Mechanics and Gas Dynamics. Purdue University. August 16, 2010.
- [13] Mechanical Seals in Centrifugal Pumps. ” *www.advantageengineering.com*. Advantage Engineering, Inc. 2014.



## APPENDIX A



John Joseph Taylor  
 Graduate Thesis

MCCF UTPA



<PITOT_TUBE>	
DARPA_POWERSWIM	
2014	

John Joseph Taylor  
Graduate Thesis

MECF

UTPA

Sting Mount:  
Mounts the C-Strut - Water Tunnel

Adapter:  
Connects the C-Strut to the Sting Mount

C-Strut:  
Enables the User to rotate model  $\angle 90^\circ$   
Guided by insert screw through slit  
Held with locking screws

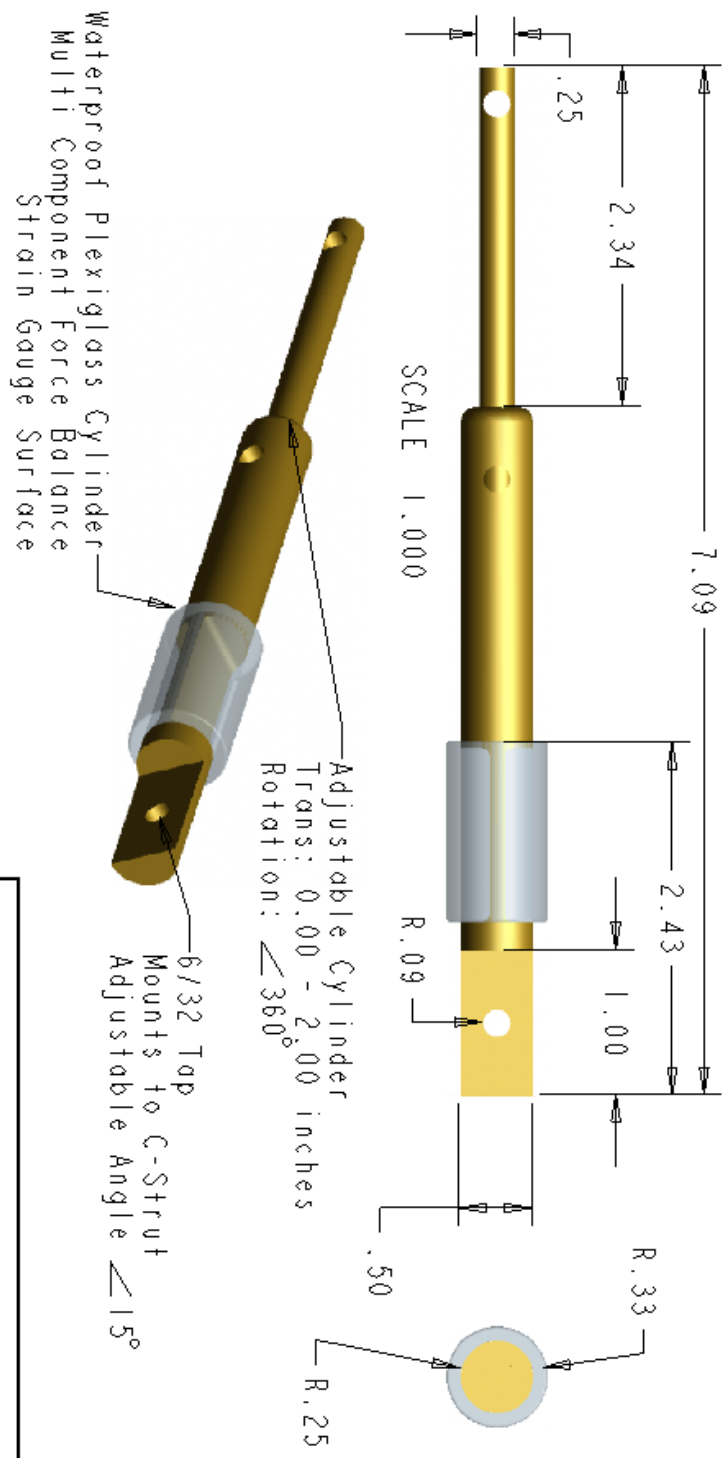
SCALE 0.400



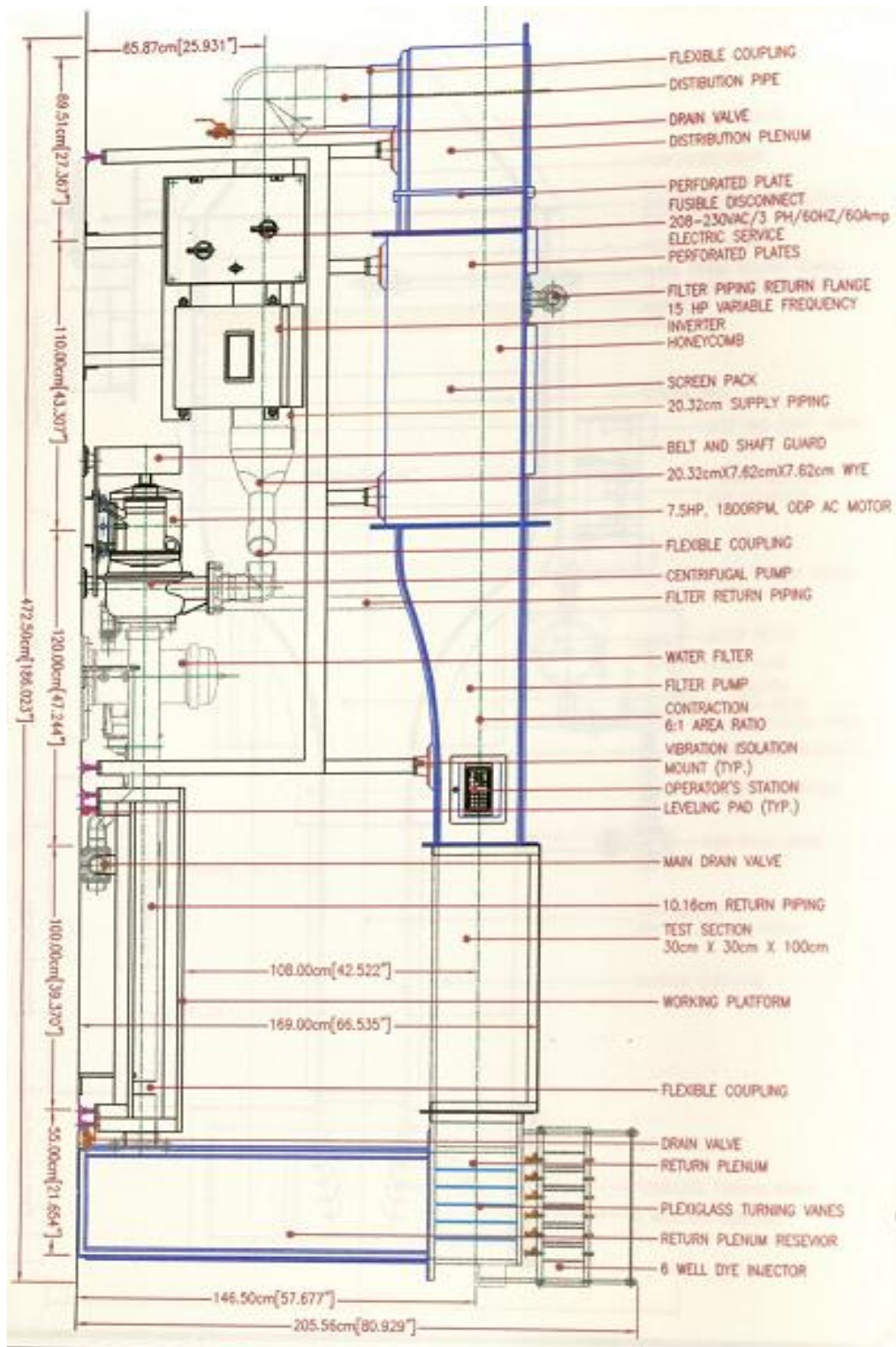
<<C\_STRUT>

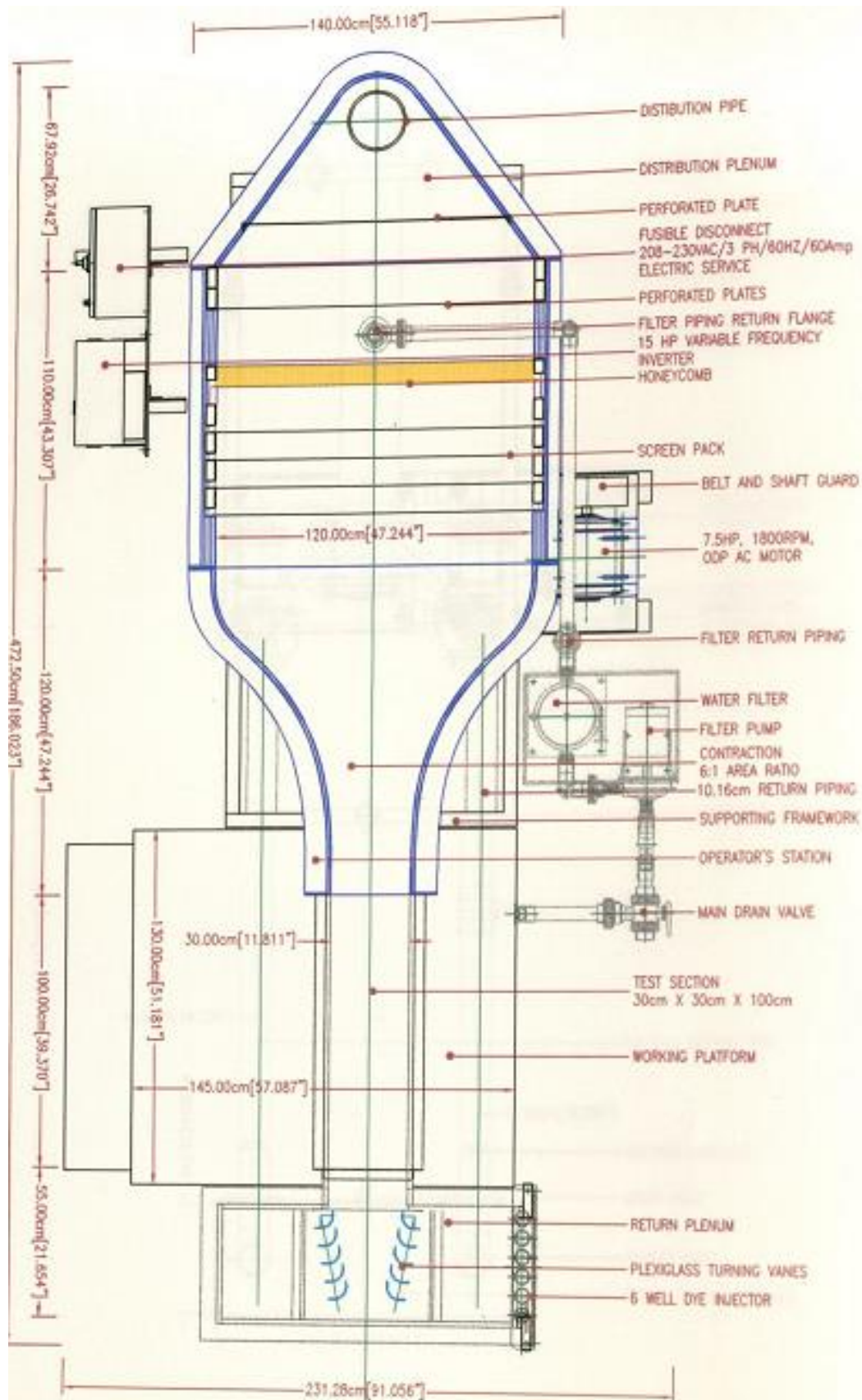
DARPA \_POWERSWIM

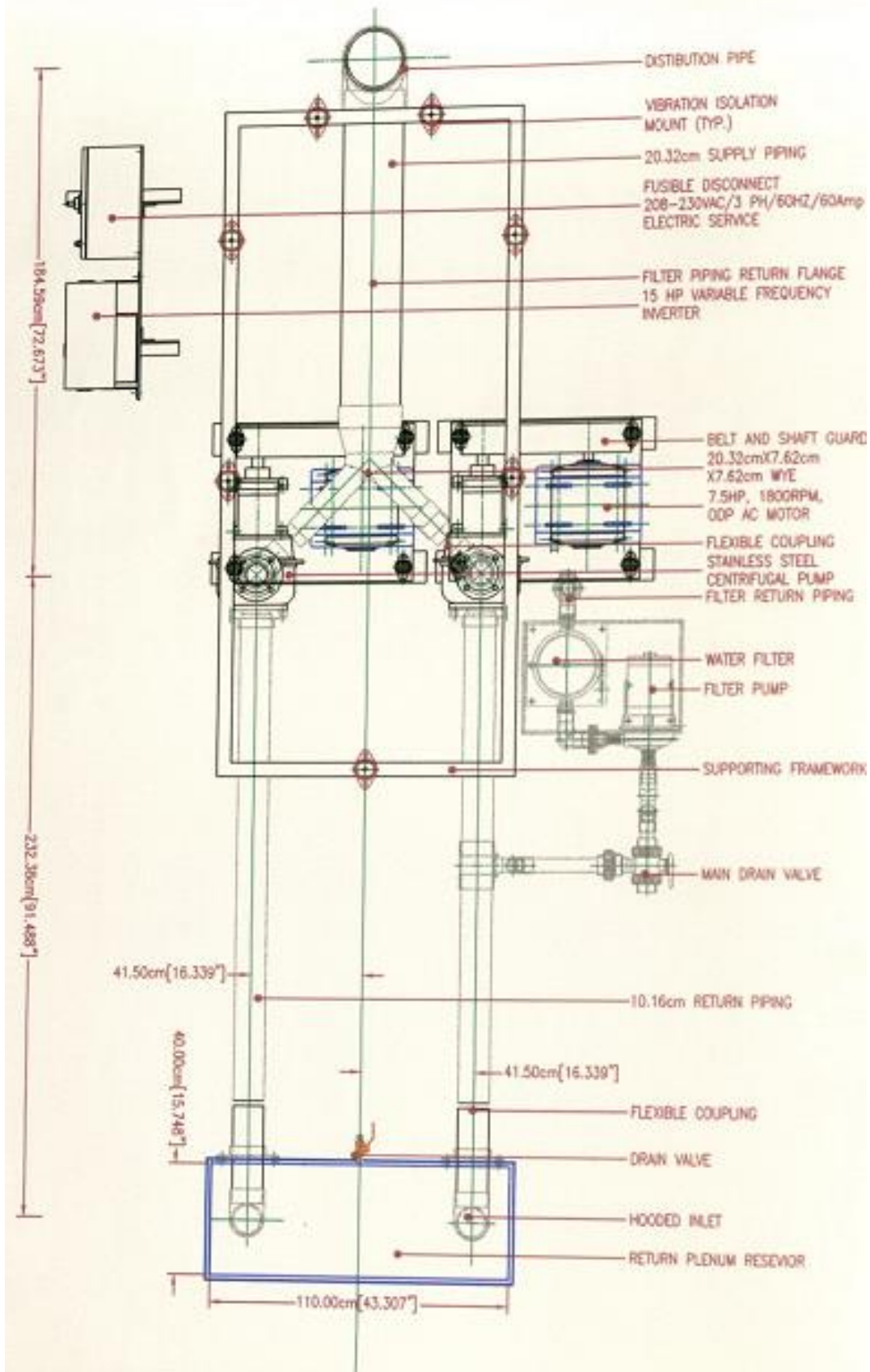
2014

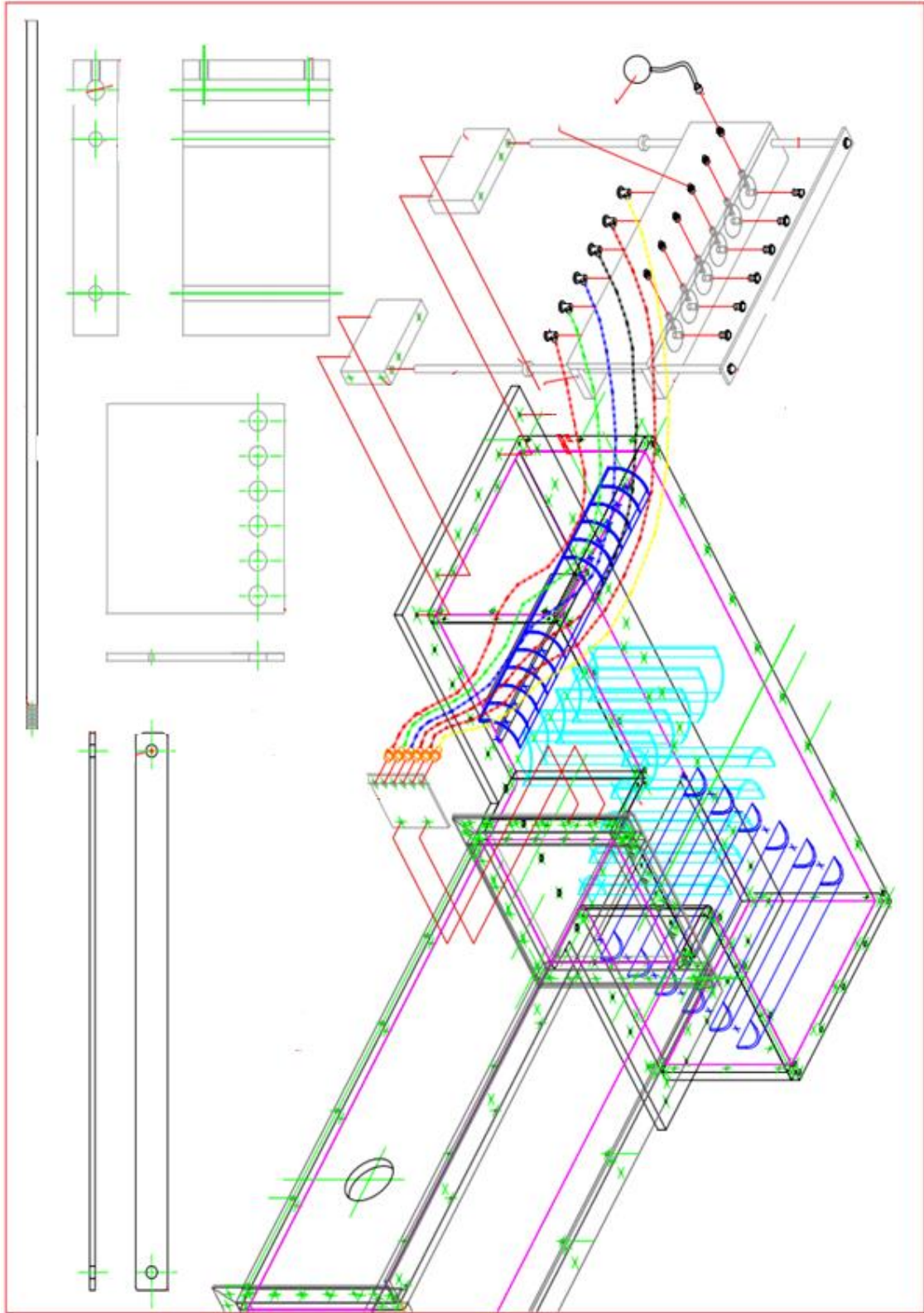


<ADJUSTABLE_FRAME>	
DARPA _POWERSWIM	
2014	

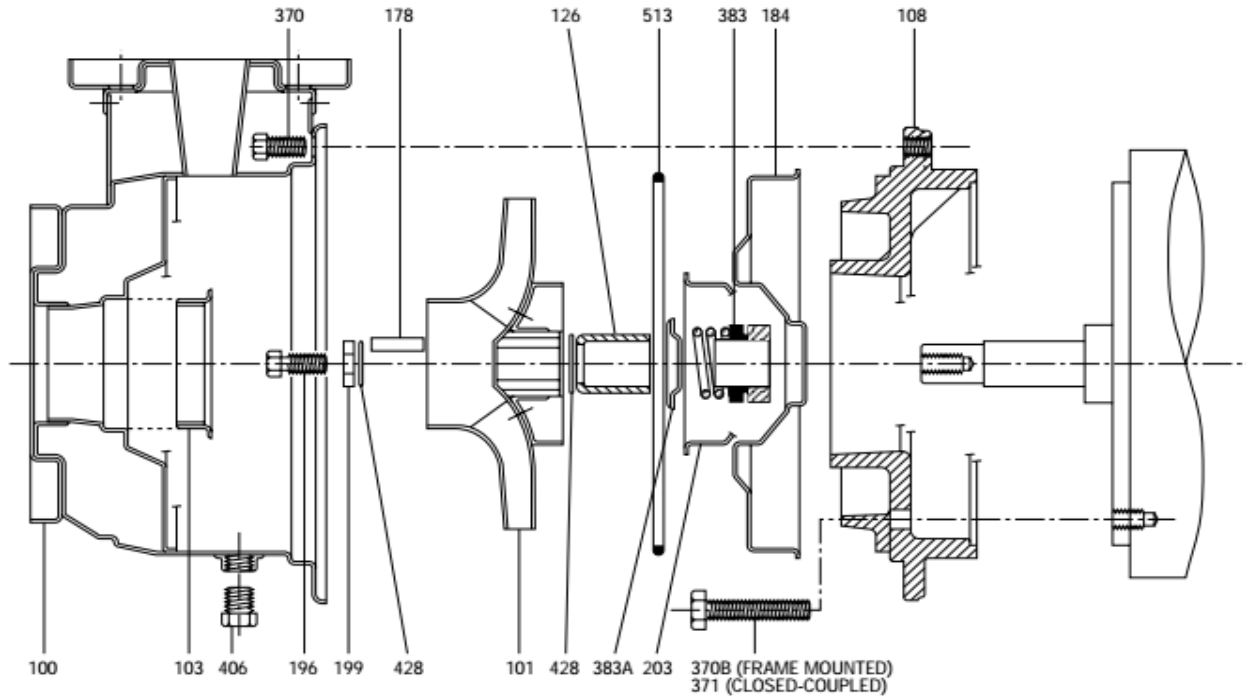












**FASTENER SIZING KEY –  
NOMINAL SIZE/TYPE/LENGTH**

13L38	3/8" Socket head x 3/4" lg.
13L40	1/2" Hex head x 2 1/4" lg.
13L41	1/2" Socket head x 1 3/4" lg.
13L43	3/8" Hex head x 2 1/4" lg.
13L86	1/2" Hex head x 1 1/4" lg. with 1/2" nut

Item No.	Part Description	Materials
100	Casing with wear ring	AISI type 304 SS
101	Impeller	
103	Wear ring, casing	
184	Seal housing (includes wear ring as noted)	
203	Wear ring, seal housing	
126	Shaft sleeve	AISI type 300 SS
178	Impeller key	
196	Impeller bolt	
199	Impeller washer	
106	Adapter for close-coupled (104JM-180JM) and S-group power frame Adapter for close-coupled (210JM-250JM motors)	Cast iron ASTM A48 CL20
370	Casing bolting (8) required	AISI type 300 SS
371	Adapter bolt (4) required for close-coupled	Carbon steel SAE 1200 series
370B	Adapter bolt for frame mounted	
383	Mechanical seal standard duty	Carbon/ ceramic
	Mechanical seal high temperature	Carbon/ Ni-resist
	Mechanical seal chemical duty	Carbon/ ceramic
	Mechanical seal severe duty/high temp.	Carbon/ tung. carb.
383A	Seal spring retainer	AISI type 300 SS
408	Drain plug 3/4" plug	
428	Impeller gasket set	Mylar
513	O-ring – casing	BUNA-N
	O-ring – casing (optional)	Viton

## BIOGRAPHICAL SKETCH

John J. Taylor, born on “el dia de los muertos” or “the day of the dead” November 2, 1988 in McAllen, Texas graduated from McAllen High School 2007, received a Bachelor’s of Science in Mechanical Engineering in 2011 from the University of Texas Pan American. During college attended summer internships at Rice University for the Catalysis and Nanomaterials Laboratory. In 2008 worked on a project “Catalyze Trichloroethylene with Zirconia Nanoparticles” and in 2010 published “Water-Phase Synthesis of Cationic Silica/Polyamine Nanoparticles.” Master of Science in Mechanical Engineering. For contacting information email at [john.taylor.7501@gmail.com](mailto:john.taylor.7501@gmail.com).